Master in Chemical Engineering

# *Synthesis of chemicals with pharmaceutical interest using green technologies*

## Master Dissertation

by

**Bernardo Sousa Pinto Rosa**

**Developed within the course of Dissertation**

based on experimental work performed at the Associate Laboratory

**Laboratory of Separation and Reaction Engineering - Laboratory of Catalysis and Materials**


Supervisor: **Prof. Dr. Joaquim Luís Bernardes Martins de Faria**

Co-supervisor: **Dr. Cláudia Sofia Castro Gomes da Silva**

U.PORTO
FEUP FACULDADE DE ENGENHARIA
UNIVERSIDADE DO PORTO

## Departament of Chemical Engineering

**September 2016**

**“*What lies behind us and what lies ahead of us***

***are tiny matters compared to what lies within us.*"**

**Henry Stanley Haskins**

# Agradecimentos

Este trabalho não seria possível sem a contribuição de algumas pessoas.

Em primeiro lugar, ao meu orientador, o Professor Doutor Joaquim Faria, pela supervisão do trabalho, contributo científico e simpatia.

À minha co-supervisora, a Doutora Cláudia Silva, pela perseverança e ajuda imprescindível em partes fulcrais deste trabalho, e por todo o aconselhamento a nível profissional e pessoal, que certamente contribuiram para a minha formação. Também pela excecional paciência que teve comigo nesta curta viagem.

Ao Professor Doutor José Luís Figueiredo por ter disponibilizado todos os recursos técnicos do Laboratório de Catálise e Materiais, do qual é director.

A todos os meus colegas de laboratório, em especial à Maria José Lima, Eliana Silva e Ana Rita Lado, por toda a disponibilização para ajudar a nível de funcionamento de equipamento e paciência. Também ao Nuno Moreira, pelo fornecimento dos LEDs. *And of course, Salma Tabassum for being a good friend and supporter.*

Aos meus amigos e às pessoas especiais da minha vida, por estarem sempre presentes, por me ouvirem e partilharem os meus bons e maus momentos.

A toda a minha família, especialmente aos meus pais pelo apoio incondicional e motivação. Obrigado por serem o meu pilar.

Por fim, a todos os que estiveram presentes de uma forma ou outra, apresentaram apoio ou companheirismo.

Sinto-me com sorte por vos ter presente na minha vida. Sem vocês nada seria o mesmo.

---

This work was partially financed by Project POCI-01-0145-FEDER-006984 – Laboratório Associado LSRE-LCM – financed by Fundo Europeu de Desenvolvimento Regional (FEDER), by COMPETE2020 – Programa Operacional Competitividade e Internacionalização (POCI) and by national funds through the Fundação para a Ciência e a Tecnologia.



# Abstract

Preservation of the environment is a very present theme in our current lifes. The pharmaceutical and chemical companies are normally seen as threatening to several ecosystems and the beings that reside in them, by fabricating their products unsustainably and polluting the surrounding environment. Yet, there is more than it looks to this, since when the concepts of green chemistry are applied, they become part of the solution, instead of part of the problem.

The Sun is the main source of energy for planet Earth, by being capable of supplying, in just one day, the global energetic necessities of 27 years. Since the contemporary energetic need is extremely high, it is favorable to choose this clean and infinite source over non-renewable sources. One way of exploring this energetic spring is through the use of light to activate chemical processes. Heterogeneous photocatalysis consists on the promotion of chemical processes, using materials known as photocatalysts, which are materials with semiconductor properties, and utilizing light as process propulsor.

Benzhydrol is a chemical compound and a pharmaceutical intermediary of antihistamines or antiallergenic and antihypertensive agents, being also a compound of interest for the perfumery industry. Benzhydrol can be synthesized via benzophenone photoreduction.

Having these facts in mind, the main aim of this work is to develop efficient photoassisted processes, (including catalysts, operation parameters and photoreaction systems), for the photocatalytic production of benzhydrol from benzophenone, which is energetically efficient, operates at ambient temperature and pressure, avoids the use of hazardous solvents and hydrogen gas, while utilizing nanostructured photocatalysts, the latter being an innovation factor for this project. The photochemical reaction is widely known and was taken into account. The photocatalytic production of benzhydrol will be studied using titanium dioxide (a semiconductor) from Evonik® Degussa ($TiO_2$ P25) under UV-LED irradiation, due to its high photostability, chemical inertness and relative low cost. However, this photocatalyst is mostly active under UV conditions and its photonic efficiency is greatly affected by the high yield of electron/hole recombination. One strategy used for increasing $TiO_2$ efficiency is by noble metal loading.

The effect of several operation parameters on the efficiency of benzhydrol production were evaluated, namely the presence of a $TiO_2$ catalyst, catalyst load, potassium hydroxide (KOH) concentration, solvent type and irradiance. The results were evaluated in terms of benzophenone conversion, yield and selectivity toward benzhydrol production. Catalysts such as noble metal (Au, Pt and Pd)-loaded $TiO_2$ P25, a $TiO_2$ material from Sigma-Aldrich and graphitic carbon nitride were also tested for the photocatalytic production of benzhydrol. In addition, the possibility of producing benzhydrol under solar simulated light was assessed.

The optimal catalyst load for $TiO_2$ P25 from Evonik® Degussa was found to be 0.1 g $L^{-1}$. The presence of KOH, appears to be crucial for enhanced yield and selectivity toward benzhydrol. A significant contribution of the pure photochemical reaction was also confirmed. Isopropanol (iPrOH) appears to be the best alcoholic solvent, also acting as hole scavenger for the selective photocatalytic production of benzhydrol. Worth noting that the efficiency of the photocatalytic reaction is directly proportional to the irradiance of the light source.

In the presence of KOH, the best results were achieved using $TiO_2$ P25 from Evonik® Degussa, with a catalyst load of 0.1 g $L^{-1}$, a KOH concentration of 5 mM, and in iPrOH as solvent (also acting as hole scavenger), reaching a selectivity of 100% and a yield of 54%, which is over 25%, in both these parameters, than the corresponding photochemical reaction. In the absence of KOH, the best performing catalyst was Pd-loaded $TiO_2$ P25, with a catalyst load of 1 g $L^{-1}$ and using iPrOH as solvent, achieving a selectivity of 25% and 22% yield, which is 10% beyond the photochemical reaction. The reaction under simulated solar light is rather effective, with the presence of KOH being crucial for the selective production of benzhydrol.

**Keywords:** Heterogeneous photocatalysis, titanium dioxide, cocatalysts, benzophenone, benzhydrol.

# Resumo

A preservação do meio ambiente é um tema muito presente nas nossas vidas. A indústria farmacêutica e química são normalmente vistas como ameaçadoras aos vários ecossistemas e aos seres que residem nestes, ao fabricarem os seus produtos de uma forma insustentável e causando poluição no meio envolvente. No entanto, isto tem mais que se lhe diga, pois quando os conceitos da química verde são postos são aplicados, passam a fazer parte da solução em vez do problema.

O sol é a principal fonte de energia do planeta Terra, sendo capaz de preencher, em apenas um dia, as nossas necessidades energéticas globais correspondentes a 27 anos. Como a procura atual energética é extremamente elevada, torna-se favorável utilizar esta fonte limpa e inesgotável, em prol das fontes não renováveis. Uma forma de exploração desta energia é através a utilização de luz para ativação de processos químicos. A fotocatálise heterogénea consiste na promoção desses processos químicos, empregando materiais denominados de fotocatalisadores, que são materiais semicondutores, utilizando a energia luminosa como impulsionadora do processo.

O benzidrol é um composto químico intermediário de fármacos, incluindo antihistamínicos ou antialergénicos e agentes antihipertensores, tendo também interesse na área dos perfumes. Este pode ser sintetizado via fotoredução da benzofenona.

Tendo estes factos em mente, o principal objetivo deste trabalho é desenvolver processos foto-assistidos eficientes (incluindo catalisadores, parâmetros de operação e sistemas de fotoreação), para a produção fotocatalítica do benzidrol a partir da a partir da benzofenona, uma vez que trata de ser energeticamente eficiente, operar a temperaturas e pressões ambientes, evitando a utilização de solventes agressivos e de hidrogénio gasoso, e faz uso da fotocatalisadores nanoestruturados, que são alvo de investigação e constituem um fator de inovação para este projeto. A reação fotoquímica é amplamente reconhecida e foi tida em conta. A produção fotocatalítica do benzidrol foi feita empregando dióxido de titânio (um semicondutor) da Evonik® Degussa ($TiO_2$ P25), sob irradiação UV-*LED*, que possui elevada fotoestabilidade, é inerte quimicamente e é de relativo baixo custo. No entanto, este principalmente está ativo em condições UV e a sua eficiência fotónica é largamente afetada pela forte recombinação entre electrões e lacunas energéticas. Uma estratégia para incrementar a eficiência deste semicondutor é através da utilização de metais nobres como co-catalisadores, depositando-os sobre a superfície do $TiO_2$.

Estudou-se o efeito que vários parâmetros têm na eficiência da produção de benzidrol, tais como a presença de catalisador de $TiO_2$, carga de catalisador, concentração de hidróxido de potássio (KOH), tipo de solvente e irradiância. Os resultados foram avaliados de acordo com a conversão de benzofenona, rendimento e seletividade relativamente à manufactura de benzidrol. Catalisadores como metais nobres (Au, Pt e Pd) – depositados na superfície de $TiO_2$ P25, um material de $TiO_2$ proveniente da Sigma-Aldrich e nitreto de carbono grafítico foram do mesmo modo estudados. Adicionalmente fizeram-se ensaios para analisar a possibilidade de produzir benzidrol sob ação de um simulador solar.

A carga ótima de catalisador para o $TiO_2$ P25 da Evonik® Degussa foi de 0.1 g $L^{-1}$. A presença de KOH parece ser crucial para potenciar o rendimento e seletividade no sentido do benzidrol. Uma contribuição

significativa da reação fotoquímica pura foi também confirmada. Isopropanol (iPrOH) parece ser o melhor solvente alcoólico e captador de lacunas energéticas para a produção seletiva fotocatalítica de benzidrol. Vale a pena notar que a eficiência da reação fotocatalítica é diretamente proporcionalà irradiância da fonte luminosa.

Na presença de KOH, os melhores resultados foram conseguidos usando $TiO_2$ P25 da Evonik® Degussa, com uma carga de catalisador de 0.1 g $L^{-1}$, concentração de KOH de 5 mM, e iPrOH como solvente (e captador de lacunas energéticas), atingindo uma seletividade de 100% e um rendimento de 54%, que é 25% superior à reação fotoquímica correspondente, nestes dois parâmetros. Já para a as reações na ausência de KOH, um desempenho superior foi conseguido para o catalisador de Pd sobre $TiO_2$ P25, com uma carga de catalisador de 1 g $L^{-1}$, fazendo também uso do iPrOH como solvente, atingindo-se uma seletividade de 25% e um rendimento de 22%, que é 10% para lá da reação fotoquímica respectiva, nestes dois parâmetros. A reação sob luz solar simulada é relativamente eficiente, com a presença de KOH a ser determinante para a produção seletiva do benzidrol.

**Palavras Chave:** Fotocatálise heterogénea, dióxido de titânio, cocatalisadores, benzofenona, benzidrol.

# Declaração

Declara, sob compromisso de honra, que este trabalho é original e que todas as contribuições não originais foram devidamente referenciadas com identificação da fonte.

---

*Bernardo Sousa Pinto Rosa*

*Porto, 1 de Setembro de 2016*

# Index

# List of Figures

# List of Tables

# Notation

### *Variables*

| | | |
|---|---|---|
| $r_{\mathrm{i,BP}}$ | Initial Benzophenone degradation rate | mM $min^{-1}$ |
| $r_{\mathrm{i,BH}}$ | Initial Benzhydrol formation rate | mM $min^{-1}$ |
| S | Selectivity | % |
| X | Conversion | % |
| Y | Yield | % |

### *Greek letters*

| | | |
|---|---|---|
| $\lambda$ | Wavelength | nm |
| $v$ | Frequency | $s^{-1}$ |

### *Roman letters*

| | | |
|---|---|---|
| $S_{BET}$ | Brunauer-Hemmett-Teller Specific Surface Area | $m^2\,g^{-1}$ |

### *Acronym list*

| | |
|---|---|
| ATR | Atenuated Total Reflectance |
| Au/P25 | Gold nanoparticles loaded on $TiO_2$ P25 from Evonik® Degussa |
| BET | Brunauer–Emmett–Teller |
| BH | Benzhydrol or Diphenylcarbinol |
| BP | Benzophenone or Diphenylketone |
| BPC | Benzopinacol or 1,1,2,2-tetraphenylethane-1,2-diol |
| CB | Conduction band |
| DCM | Dicyandiamide |
| $e^-$ | Electron |
| $e^-_{CB}$ | Conduction band electron |
| EtOH | Ethanol |
| FTIR | Fourier Transform Infrared |
| g-$C_3N_4$ | Graphitic carbon nitride |
| $h^+$ | Hole |
| $h^+_{VB}$ | Valence band hole |
| $H_2$ | Hydrogen |
| $H^+$ | Hydrogen ion |
| HOMO | Highest Ocuppied Molecular Orbital |
| HPLC | High Performance Liquid Chromatography |
| iPrOH | 2-propanol or isopropanol |

| | |
|---|---|
| KM | Kubelka Munk |
| KOH | Potassium hydroxide |
| LED | Light emitting diode |
| LUMO | Lowest Unoccupied Molecular Orbital |
| MA | Massachusetts |
| MeOH | Methanol |
| P25 | Titanium Dioxide P25 from Evonik® Degussa |
| Pd/P25 | Palladium nanoparticles loaded on $TiO_2$ P25 from Evonik® Degussa |
| Pt/P25 | Platinum nanoparticles loaded on $TiO_2$ P25 from Evonik® Degussa |
| SA | Titanium Dioxide from Sigma-Aldrich |
| SCE | Saturated Calomel Electrode |
| SHE | Standard Hydrogen Electrode |
| TEM | Transmission Electron Microscopy |
| UP $H_2O$ | Ultrapure water |
| UV | Ultraviolet |
| UV-Vis | Ultraviolet-Visible |
| VB | Valence band |
| Vis | Visible |
| wt.% | Weight percentage |

# 1 Introduction

## 1.1 Project presentation and framework

One of the main problems that our world faces is the obtaining of energy in a clean fashion, mainly due to the decrease in fossil fuels' reserves and the environmental issues involved in the extraction of such resources [1, 2]. The increased need for energy production arose from the industrial revolution, where a substantial burst on the human population, followed by economic exponential growth occured. This has put a considerable amount of strain on the Earth's natural resources and on the environment since then.

The Sun is a tremendous source of energy, able to provide enough clean solar energy to power up the world for 27 years in a single day [3]. It is a fundamental component to a whole range of reactions such as the oxidation of water to molecular oxygen and the fixation of $CO_2$ through natural photosynthesis, and also a necessary component to processes such as the water and carbon cycles.

The world has changed a lot due to technological advances in recent years. The development of technologies capable of converting solar energy into chemical energy constitutes an enormous challenge in the present. Two of the most important approaches taken for the storage of solar energy are through the direct conversion to electricity on photovoltaic cells, which can then be put to various uses, or through the generation of high energy fuels such as molecular hydrogen from water [4].

Photocatalytic technologies have been gaining increasing commercial interest worldwide mostly in the fields of water and air treatment, architecture, and fuels production [5-7].

Photocatalytic organic synthesis is considered at the forefront of current chemistry trends, in particular the implementation of green chemistry methods to be transferred to industry.

In parallel, due to the increasingly use of medicines, the pharmaceutical companies have been compelled to find ways to manufacture their products in larger quantities, although not always using the most sustainable technologies [8, 9]. There have been some recommended alternatives to this such as the use of less hazardous chemical synthesis routes, safer solvents, higher energetically efficient processes, inherent safer chemistry, while maintining low cost and environmental impact to a minimum, following the twelve principles of green chemistry [10].

Benzhydrol (BH) is a chemical compound and a pharmaceutical intermediary in the synthesis of antihistamines, antihypertensive and antiallergenic agents. It is also a compound of interest for the perfumery industry. It can be synthesized via benzophenone (BP) photoreduction, although usually it is currently produced via hydrogenation of BP using different catalysts.

The present work is focused on the production of BH by photocatalytic reduction of BP.

Although the pure photochemical route for BH production from BP has been reported in previous studies [11-21], this reaction normally yields other products such as the corresponding pinacol, the benzopinacol (BPC) [20], lacking in selectivity toward BH. On the other hand, the the photocatalytic route remains quite unexplored. Compared with the process currently utilized in the industry, the photo-assisted production of BH presents an array of advantages such as the possibility of using a renewable energy source, like the

Sun, making it energetically more efficient [22], operating at ambient temperatures and pressure, avoiding the use of environmentally aggressive solvents , while making use of nanostructured photocatalysis [23].

## 1.2 Aim of the Dissertation

The current dissertation aims at developing efficient photo-assisted processes, including catalysts and photoreaction systems, for the production of BH from BP.

Photocatalytic organic synthesis presents several advantages over traditional organic synthesis methods such as the use of mild conditions of temperature and pressure, while avoiding hazardous solvents and aggressive oxidant agents. Moreover, nanotechnology, being the capability to fabricate new structures at atomic scale, allows the development of novel photocatalytic materials. Solar radiation is a cheap, clean and available energy source throughout the globe [24]. The Sun's visible light makes about 43% of the total radiation spectrum that hits the earth´s surface, while the ultraviolet radiation ranges from 3-6% [25]. Therefore, it is of core interest to perform and viabilize this reaction into visible light, while there is little to none known reports of this [23]. Although photocatalytic organic synthesis can be virtually carried out under solar irradiation, technological implementation and reproducibility of conversion and selectivity can be a hard task. In this view, LED-assisted photoreactors can be considered an energy-efficient and highly reliable option.

The specific objetives estabilished for this work are:

1. The synthesis and characterization of photocatalysts, mostly based on $TiO_2$, noble metal (Pt, Pd and Au)-loaded $TiO_2$ and graphitic carbon nitride;
2. Photochemical and photocatalytic reduction of BP to selectively form BH under UV-LED irradiation;
3. To study the effect of operating parameters such as solvent, type of catalyst, catalyst load and irradiance;
4. To assess the possibility of producing BH under solar light irradiation.

## 1.3 Thesis Outline

The dissertation is organized in five chapters.

Chapter 1 gives a brief introduction to the topic under study in the present dissertation. It also elaborates on the objectives and thesis outline.

Chapter 2 contextualizes photocatalysis, existing technologies and catalysts within the field on photoinitiated reactions. It also addresses the initial compound, the desired and the undesired products that are expected from the elected reaction.

Chapter 3 elucidates a brief technical description of the equipment and materials used.

Chapter 4 presents the results of the catalysts characterization and the performed experiments, while discussing the results obtained during this work.

Chapter 5 presents the conclusions that were taken from this study, along with some limitations encountered along the way, while specifying some suggestions for further project development.

# 2 State of the Art

Green chemistry is a relatively new emerging field that strives to work at the molecular level to achieve sustainability [10]. In recent years, photocatalytic technology is growing to be one of the most effective and sustainable strategies for resolving environmental pollution issues [26]. In parallel to the plants ability to act as light sensitive chemical factories [6], solar energy is the ultimate green alternative to enable chemical transformations [27], since it stands out as the most promising choice to meet the current energy demand due to its plentiful, clean, and renewable features and shows great potential for driving environmentally benign chemical transformations [28]. These developments brought the promising alternative of capture and usage of solar energy through p-n junction solar cells of photovoltaic devices that currently have a limited conversion efficiency of 34% [29]. Moreover, in the last year, the minute amount of 0.66% of the total electricity produced comes from solar energy while on the industrial sector, energy consumption is below the minimum accountable amount [30, 31].

The use of light irradiation shifts the thermodynamic emphasis from performing high-temperature chemical reactions to doing so at ambient conditions, which thus avoids unwanted byproducts formed at elevated temperatures, is driven by clean renewable energy sources and limits environmental impact [32].

Photocatalysis has been used on a broad range of research areas, such as water splitting, $CO_2$ reduction, water treatment, among others [33]. Figure 1 shows the relevance of photoinitiated processes and its benchmark photocatalyst on the scientific community.

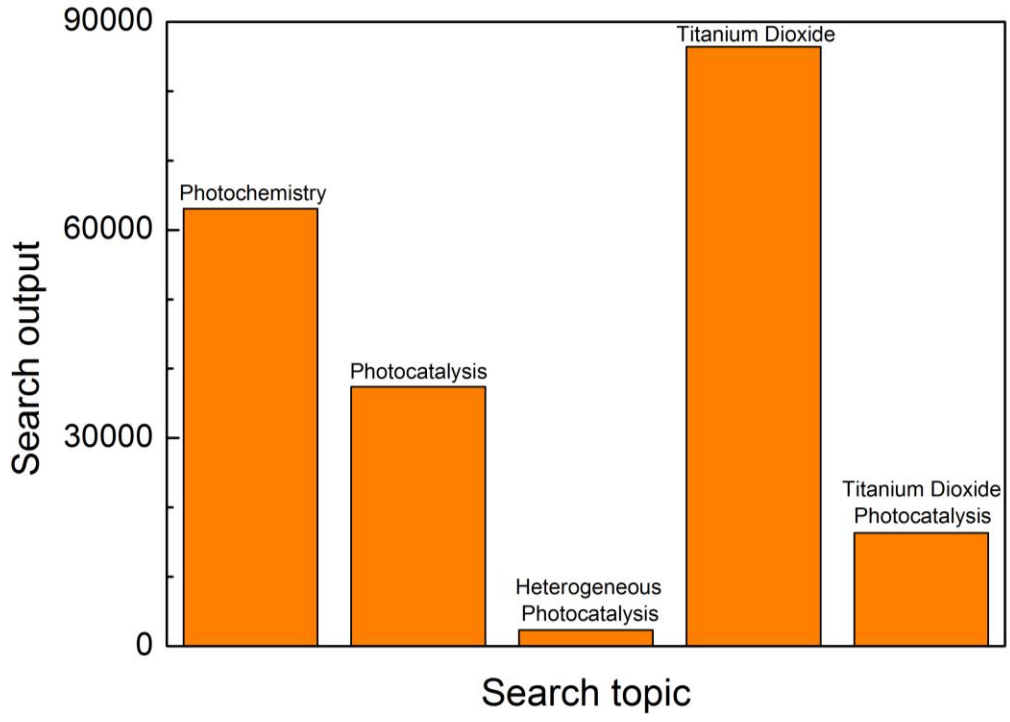


**Figure 1 -** Number of results for research papers from Scopus for the designated document search inputs, as of 6 of June of 2016. The search outputs range from the year 1900 until the moment of the search.

Although heterogeneous photocatalysis has expanded rapidly due to various developments, particularly in the design and production of new photocatalysts and their applications [28, 32], further study is needed for a wider scale use.

## 2.1 Heterogenous Photocatalysis

Photocatalysis is the acceleration of a photoinitiated reaction with the use of a catalyst [34] which can be on the same phase as the reactants, being homogeneous or in a different phase - heterogeneous photocatalysis. Heterogenous photocatalytic reactions can take place in various media: gas phase, pure organic liquid phases or aqueous solutions [35]. The advantages over homogeneous photocatalysis consists mostly on the possibility of catalyst recovery and easier separation of the reaction products, so providing a greener way for organic chemical transformations [5].

Since Fujishima and Honda's report on water photolysis using a semiconductor electrode in 1972 [36], heterogeneous photocatalysis became an active area of research on a variety of fields [7]. Currently, most of the aplications of heterogeneous photocatalysis deal with the following topics [22]:

1. Transformation of light energy into more easily stored and used chemical energy, such as hydrogen production from water photolysis;
2. Unselective degradation of undesired chemicals, such as pollutants of different sources through molecular oxygen rather than hazard chemical oxidants;
3. Using light for activating a selective chemical process, such as the one this work is focused on.

Many works on the efficiency of the titanium dioxide ($TiO_2$), the benchmark catalyst in photocatalytic applications, by UV-Vis radiative activation have been reported [5, 37-40]. In essence, during an heterogeneous photocatalytic reaction there is the activation of the catalyst particles, rather than the substrate that is adsorbed at the surface of the solid material. For the catalyst to be efficient, it should present semiconductive properties and have such a band gap that allows for the oxidation and reduction of the desired compounds. The semiconductor should be stable under the operation conditions.

Heterogeneous photocatalysis in organic synthesis became obvious from the moment that selective reactions of organic and other inorganic substrate could also be induced by band gap irradiation of a variety of semiconductor particles [35].

By means of incident light with energy matching or greater than the band gap energy of the given semiconductor, an electron ($e^-$) from an electron-filled valence band (VB, Highest Occupied Molecular Orbital - HOMO) is excited to a vacant conduction band (CB, Lowest unoccupied Molecular Orbital - LUMO), leaving a positive hole ($h^+$) in the VB (Figure 2). From here, two situations may happen. In the absence of suitable electron and hole scavengers, the excited electrons and holes tend to recombine very quickly, dissipating the energy as heat. However, if a suitable scavenger or surface defect is accessible to trap the photogenerated electrons or holes, recombination is scarce and further redox reactions may occur. That is, due to their electronic structures, heterogeneous photocatalysts can act as mediators in chemical redox processes, by overcoming high activation energies under mild conditions [22]. This is because valence band holes ($h^+_{VB}$) are powerful oxidants, whereas conduction band electrons ($e^-_{CB}$) are

reductants and so these photogenerated electrons and positive holes drive reduction and oxidation, respectively, of different compounds [41].

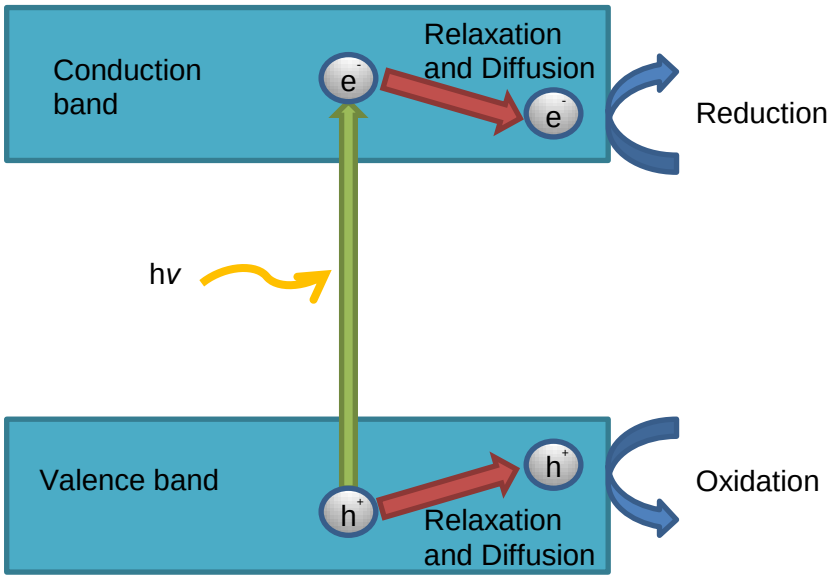


**Figure 2 -** Schematic representation of the basic photocatalytic process upon radiation absorption, adapted from Nakata et al. [42].

## 2.2 Titanium dioxide photocatalyst

On the topic of photocatalysis, several different materials are utilized as semiconductors for photocatalytic reactions. A few examples of these are gold nanoparticles [43], chalcogenides such as zinc oxide [44] and cadmium sulfide (CdS) [45-47], and $TiO_2$. Moreover, due to the plethora of developed studies since Fujishima and Honda's report on water photolysis using a semiconductor electrode in 1972 [36], and its array of advantages when compared to other materials, $TiO_2$ has been considered to be the benchmark photocatalyst. Besides, it has the potential of inducing reductive chemical transformations efficiently [38], as intended for this work.

$TiO_2$ has many applications, ranging from commercial products, such as pharmaceuticals, drugs and sunscreens, to solar cells and is used as mediator in several reactions [48]. Its high photostability, inertness on hazardous conditions, plus the highly reactive surface excited electrons and holes that will be responsible for the redox reaction for heterogeneous photocatalysis are what makes it interesting when comparing to other known semiconductors [5, 49].

Nevertheless, $TiO_2$ possesses a high electron-hole recombination rate and it is only active under UV irradiation conditions, which represents about 3-6% of the solar spectrum [25]. These are a few drawbacks that are to be considered, and limit its wider commercial application.

Considering the delineated objetive of employing solar energy, it is favorable to increase the radiation range that activates $TiO_2$ toward longer wavelengths, since 43% of the solar spectrum is located under the visible light.

The three common crystal phases of titanium dioxide are brookite, rutile and anatase. These two latter phases have a large band gap, of 3.0 eV for rutile and 3.2 eV for anatase against a standard hydrogen electrode (SHE) [50]. Figure 3 shows a graphical representation of anatase and rutile crystal strutures.
Still, the $TiO_2$ P25 from Evonik® Degussa powder contains a mixture of anatase and rutile in an approximately 3:1 proportion. It has been reported that this relative quantity is important to ensure the best photocatalytic properties for $TiO_2$ [51]. For all these reasons, this semiconductor $TiO_2$ P25 will be used as a starting point for the sake of this dissertation and will be compared with commercial anatase $TiO_2$ from Sigma-Aldrich (SA).

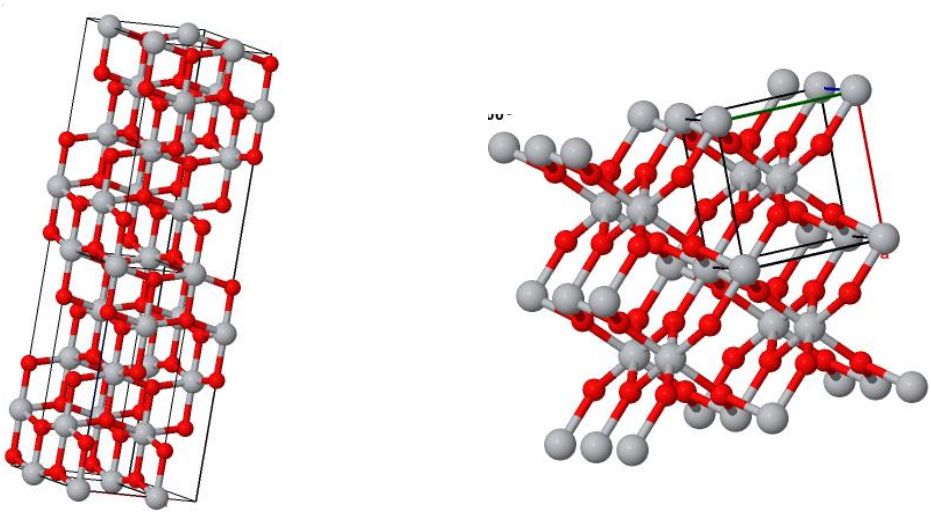

**Figure 3 -** $TiO_2$ crystal phases, with anatase (left) and rutile (right) [52]. Red and grey spheres are oxygen and titanium atoms, respectively.

Modifyings the semicondutor's surface is a known method of improving catalyst properties, either with noble metals, nonmetallic elements or with dyes [37]. The deposition of noble metal nanoparticles, such as gold (Au), platinum (Pt) and palladium (Pd), on $TiO_2$ surface may induce a synergetic effect with the metal nanoparticles acting as electron buffers, enhancing the separation efficiency of hole-electron pairs, due to its strong electron afinity [53-56], while also lowering the activation energies, trapping the charge carriers and supplying of oxidation and reduction active sites [57]. An optimal metal load should be found, since that an excessive amount of metal may cause the photocatalytic surface to be overly covered, difficulting the light absorption and delaying charge separation to occur [58]. Most commonly, the highest photoefficiencies found for metal-loaded semiconductors are generally found in the range of 0.5-2 wt.% [54, 59, 60]. Harmony between the semiconductor and noble metal should also be ensured in terms of energy levels and electronic structures [57].

## 2.3 Photocatalytic production of benzhydrol from benzophenone

Benzhydrol (BH), or diphenylcarbinol is a colorless crystalline secondary alcohol with the chemical formula $(C_6H_5)_2CHOH$ (Figure 4). It is industrially produced via hydrogenation of BP using sodium borohydride [61], palladium based catalysts on an active carbon support or even Raney Nickel [62] catalysts. It may also be obtained from phenylmagnesium bromide and benzaldehyde or with ethyl formate, via a Grignard reaction [62], and it is mainly used in organic synthesis. These processes have an array of disavantages such as the use of hydrogen and the production of diphenylmethane as occurs for the first reaction. Moreover they require hazardous and dangerous chemical reagents and emit harmful waste, while also working under high temperatures and pressures [50], with expensive catalysts.

Benzophenone (BP) or diphenylketone is a colorless crystalline ketone solid with the chemical formula $(C_6H_5)_2CO$. It has a very broad domain of functions, due to it being UV active [11-21]. It can be used as a photoinitiator in UV-curing applications [63], as a catalyst [7], as one of the components of sunscreen [64], as a fragrance enhancer or to prevent products from losing scents and colors in the presence of UV light, among others [65]. BP is persistent and bioaccumulative [66, 67], whilst linked to cancer, endocrine disruption, and organ system toxicity [68].

BH is utilized on several areas, from terminating group for polymerizations [69], fixative on perfumes, but it is mainly used as an intermediate of pharmaceuticals (including antihistamines or antiallergenic, antihypertensive and agents and even eugeroic agents), agrochemicals, and other organic compounds [70]. The benzhydril group is present in the structure of histamines such as the diphenylhydramine and is even used for the synthesis of Modafinil.

Since the original discovery of Ciamician and Silber [71] of the action of light on the reduction of BP into BH, many studies have been reported on the determination of the mechanism involved in this photoreaction [16, 20].

The proposed mechanism for the photochemical reaction [16, 20] (Appendix B, Figure B.1) includes a triplet BP that abstracts hydrogen from the alcohol, forming two ketyl radicals, the diphenyl ketyl from BP and dimethyl ketyl, in the case of isopropanol (iPrOH). From here, this radical transfers hydrogen to ground-state BP, forming a second ketone-derived radical (diphenyl ketyl) and the alcohol-derived ketone (acetone) [72]. Afterwards, dimerization of the two diphenyl ketyl radicals may occur to form benzopinacol, or new hydrogen abstraction from the alcohol or its radical may happen, producing BH [11]. From previous photochemical experiments, great amounts of pinacols have been formed, while BH is one of the residual products [73].

Benzopinacol (BPC), benzopinacone or 1,1,2,2-tetraphenylethane-1,2-diol is a diol organic compound with the chemical formula $(C_6H_5)_2C(OH)C(OH)(C_6H_5)_2$. It is a one of the-products formed from BP photoreduction, as the photoreduction of ketones with alcohols are a known method for the production of pinacols [17]. According to a patent, BPC is a known polymerization initiador [74] and is investigated for research purposes due to its fluorescence [75]. For this work, this is the only identified undesired product from the photoreduction of BP.

The UV-Vis spectra and chromatogram from the high performance liquid chromatography (HPLC) of BP, BH and BPC are presented on Figure A.1 and Figure A. 2 (Appendix A).

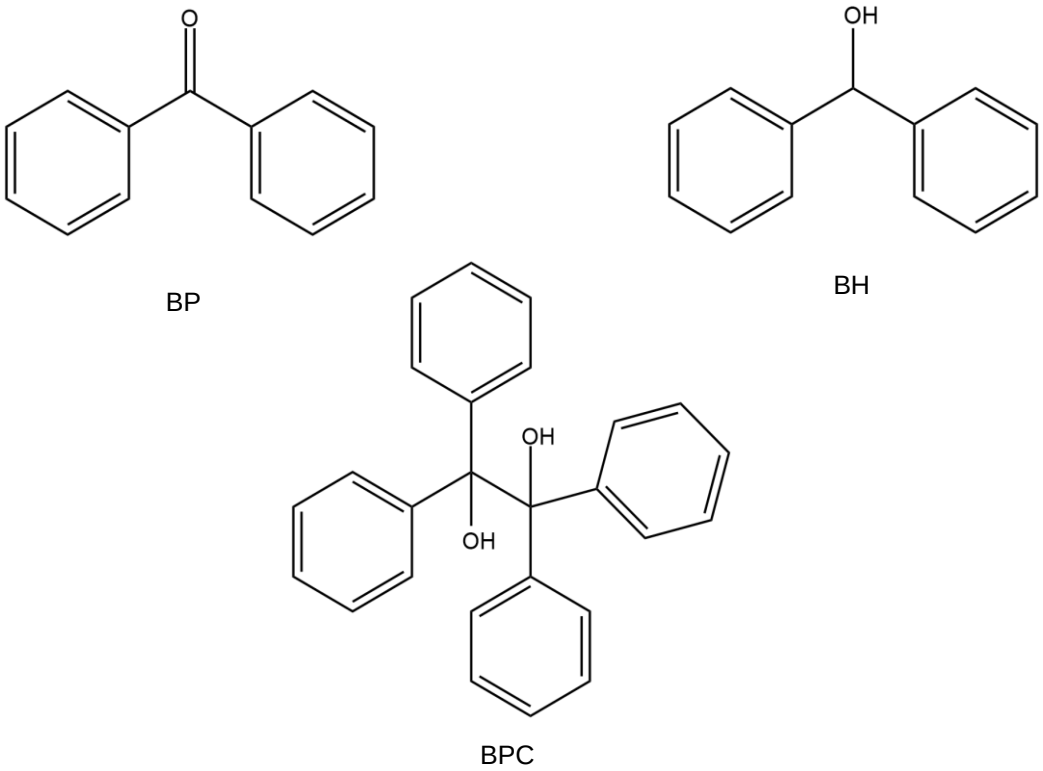


**Figure 4 -** Chemical structure of benzophenone (BP), benzhydrol (BH) and benzopinacol (BPC).

One of the first reports on the photocatalytic reduction of a carbonyl compound was authored by Cuendet and Grätzel in 1987 [76], with the hydrogenation of lactate to pyruvate under irradiation of aqueous suspension of $TiO_2$. Shiragami et al. [45-47] applied visible light to the photocatalytic reduction of BP using CdS to produce BH with a remarkable yield of an 95% over 3 hours with the remaining substrate being converted to BPC. However, a few disadvantages are to be considered, since both the solvent (methanol) and the catalyst (CdS) are considered hazardous, and a high energy lamp was used to irradiate the solution. There are very few studies of photocatalytic reduction of BP with $TiO_2$ P25 [38]. The mechanism of the photocatalytic production of BH from BP using $TiO_2$ as catalyst has been proposed by Escobar et al. [23] and includes the steps from Figure 5. Worth considering that the study published by this group performed the reaction in a short amount of time (45 minutes), but obtained a low amount of BH (40% of chromatographic area) and also employed a high energy lamp of xenon and mercury.

When $TiO_2$ is irradiated with UV radiation with the appropriate wavelength, electrons may be excited from the VB to the CB, creating electron-hole pairs on the semiconductor's surface surface, as described beforehand (Eq. 1). Under deaerated conditions, holes are quenched by an alcohol such as isopropanol (iPrOH), which is in competition with the photogenerated electrons for effective electron hole quenching [77], with formation of $H^+$ and acetone (Eq. 2). A first electron transfer to BP and hydrogenation occurs

forming a ketyl radical (Eq. 3), with a second reaction yielding BH (Eq. 4), since this is a two-photon product [19].

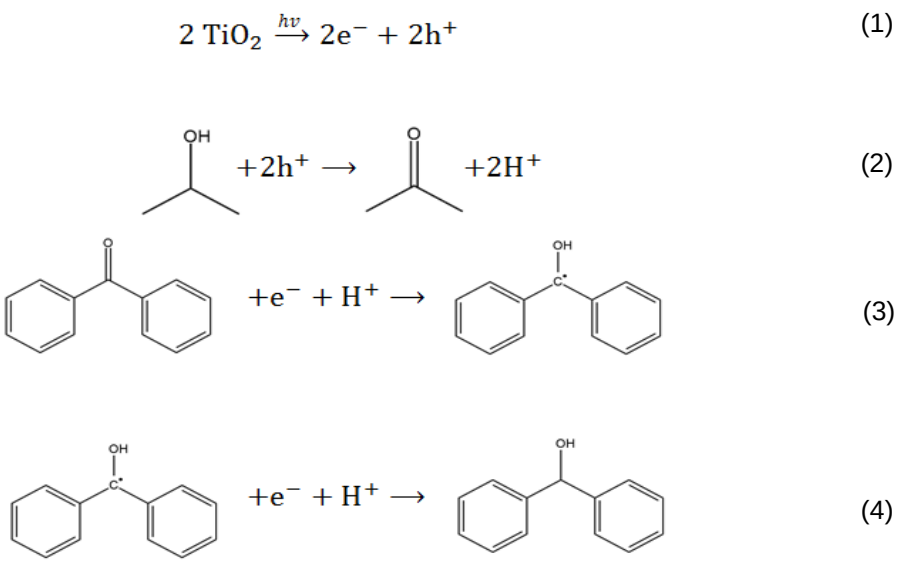


**Figure 5 -** Proposed photocatalytic mechanism for the photoreduction of BP for the production of BH.

In fact, this reaction is feasible due to the electronic properties of $TiO_2$ P25, and redox potentials of iPrOH and BP: the conduction band of both varieties of $TiO_2$ situates at c.a. -0.7 eV vs. Saturated Calomel Electrode (SCE) [78], which is lower than the BP reduction potencial toward the ketyl radical [79], and the potencial of the VB of $TiO_2$, at around 2.3 eV vs. SCE [80], is higher than that of the alcohol [81] (Figure 6). However, according to Kalinowski et al., the electrode process for a second electron transfer for BP is complicated, so that the normal redox potentials could not be measured [79].

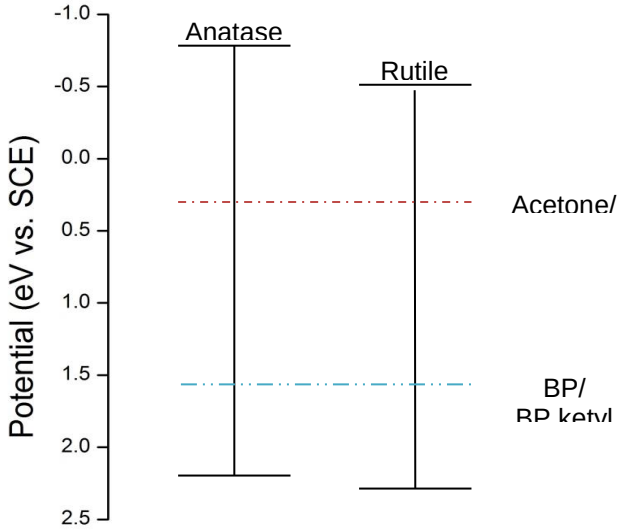


**Figure 6 -** Potential for photocatalytic reduction of BP and oxidation of iPrOH, in eV vs. Saturated Calomel Electrode (SCE) [78-81].

# 3 Experimental description

Different setups were used during this project, either for the production of BH or for the synthesis and characterization of the catalysts.

The experimental setups and respective procedures are described in this section.

## 3.1 Reagents

BP ($(C_6H_5)_2CO$, 99%) was obtained from Sigma-Aldrich. iPrOH ($C_3H_8O$, 99.5%) was obtained from Sigma-Aldrich, and potassium hydroxide (KOH) in pellets (≥86 %), was obtained from Fluka. BH ($(C_6H_5)_2CHOH$, 99%) was obtained from Fluka, and BPC ($(C_6H_5)_2C(OH)C(C_6H_5)_2OH$, 98%) was obtained from Alfa Aesar. Ethanol (EtOH, $CH_3CH_2OH$, ≥ 99.5%) was obtained from Panreac. Dicyanamide (DCM, $NaN(CN)_2$,96%), was obtained from Fluka. Gold (III) Chloride Trihydrate ($HAuCl_4 \cdot 3H_2O$,≥49%, Au basis),Palladium (II) Chloride ($PdCl_2$, 99%) and Chloroplatinic acid solution ($H_2PtCl_6$, 8 wt.% in $H_2O$) were supplied by Sigma-Aldrich.

Methanol (MeOH, $CH_4O$, ≥99.8%), used for HPLC analysis and as solvent for some reactions, was obtained from VWR. Along with it was used Ultrapure water (UP $H_2O$), which was produced in a Direct-Q Millipore system (Merck Millipore, Billerica, MA, USA).

$TiO_2$ Aeroxide® P25 powder was obtained from Evonik® Degussa Corporation (Essen, Germany) and commercial $TiO_2$ (SA, ≥99%, anatase nanopowder) from Sigma-Aldrich.

## 3.2 Catalysis Synthesis

For the production of g-$C_3N_4$, 10 g of DCM powder were put into an alumina crucible with a cover, and then heat-heated at 450 ºC in a muffle furnace for 2 hours at a heating rate of 2 ºC $min^{-1}$; after that the temperature was elevated to 550 ºC for 4 hours. Then, the sample was cooled naturally to room temperature [82].

Metals were loaded on P25 by incipient wetness impregnation method. Briefly, the photocatalyst was placed in an Erlenmeyer flask and sonicated for 30 min. Then, an aqueous solution containing the metal precursor (1 wt.% of metal) was pumped into the flask. The material was maintained under sonication for 90 min and then dried at 100 ºC for 24 hours. Finally, the catalysts were heat treated under nitrogen flow at 200 ºC for 1 hour and reduced at the same temperature under hydrogen flow for 3 hours, yielding Au/P25, Pd/P25 and Pt/P25.

## 3.3 Photocatalytic experiments

For the sake of evaluating the effect of the irradiated wavelength, two different reaction systems were used. For the study of UV light driven reactions was used a system with four high intensity UV LEDs

simetrically located at a distance of 3.5 centimeters from the reactor, making an average intensity of 613 W $m^{-2}$. The LEDs emit radiation on the UV zone, with its maximum intensity at c.a. 382 nm, as is evident from Figure 7. This wavelength was chosen due to the cost of the LEDs and the fact that $TiO_2$ is activate at this wavelength range [83]. The light intensity was measured at the outer wall of the reactor with a UV–Vis spectroradiometer (USB2000+, OceanOptics, USA).

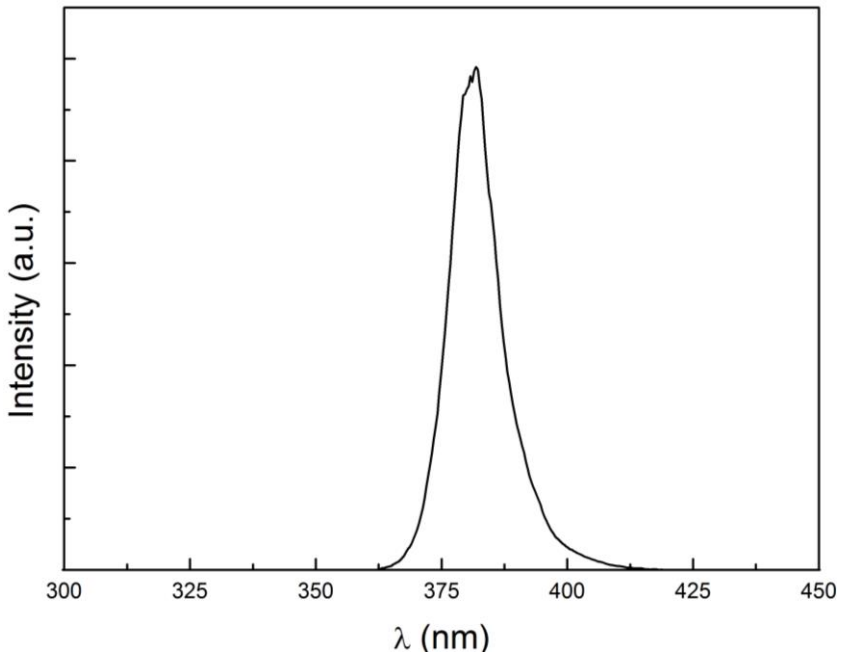


**Figure 7 –** Average spectral irradiance of the four UV LEDs.

To study the photoreduction of BP into BH, a glass immersion photochemical reator was used, located axially to the 4 LEDs. The installation was comprised of not only the photochemical reactor and the four LEDs, but also and a water cooling system, to ensure that the temperature was constant and the possible heating derived from the LEDs was properly removed. The reaction mixture's temperature has been measured with a Kane-May 330 Thermometer, confirming that it was maintained at room temperature (~20 ºC). For every experiment, a solution with the desired concentration was prepared by dissolving BP in the adequate solvent, while kept out of light. Whilst the LEDs were off, the solution was introduced in the reactor and purged with an Argon flow, adding the catalyst straight away. The flow of Argon was kept during the reaction at 15 mL $min^{-1}$. This inert gas was introduced in order to ensure that no oxygen is present in the reaction medium. The solution was left to stir for about 15 minutes so that the reaction mixture would be completetly homogeneous and the adsorption-desorption equilibrium is reached. In some cases, a small volume of a 0.1 M KOH alcoholic solution was further added to the reaction mixture. The total volume was kept at 100 mL. A sample was taken at the end of this dark phase, just before starting the irradiation, which is considered time 0.

Afterwards, the LEDs were turned on and samples were taken at specific times (5, 10, 15, 20, 30, 45 and 60 minutes). These were centrifuged and analyzed by HPLC. A photograph was taken while a reaction

was going on, as can be seen from Figure 8 a. Also, a schematic representation of the described system is also represented on Figure 8 b.

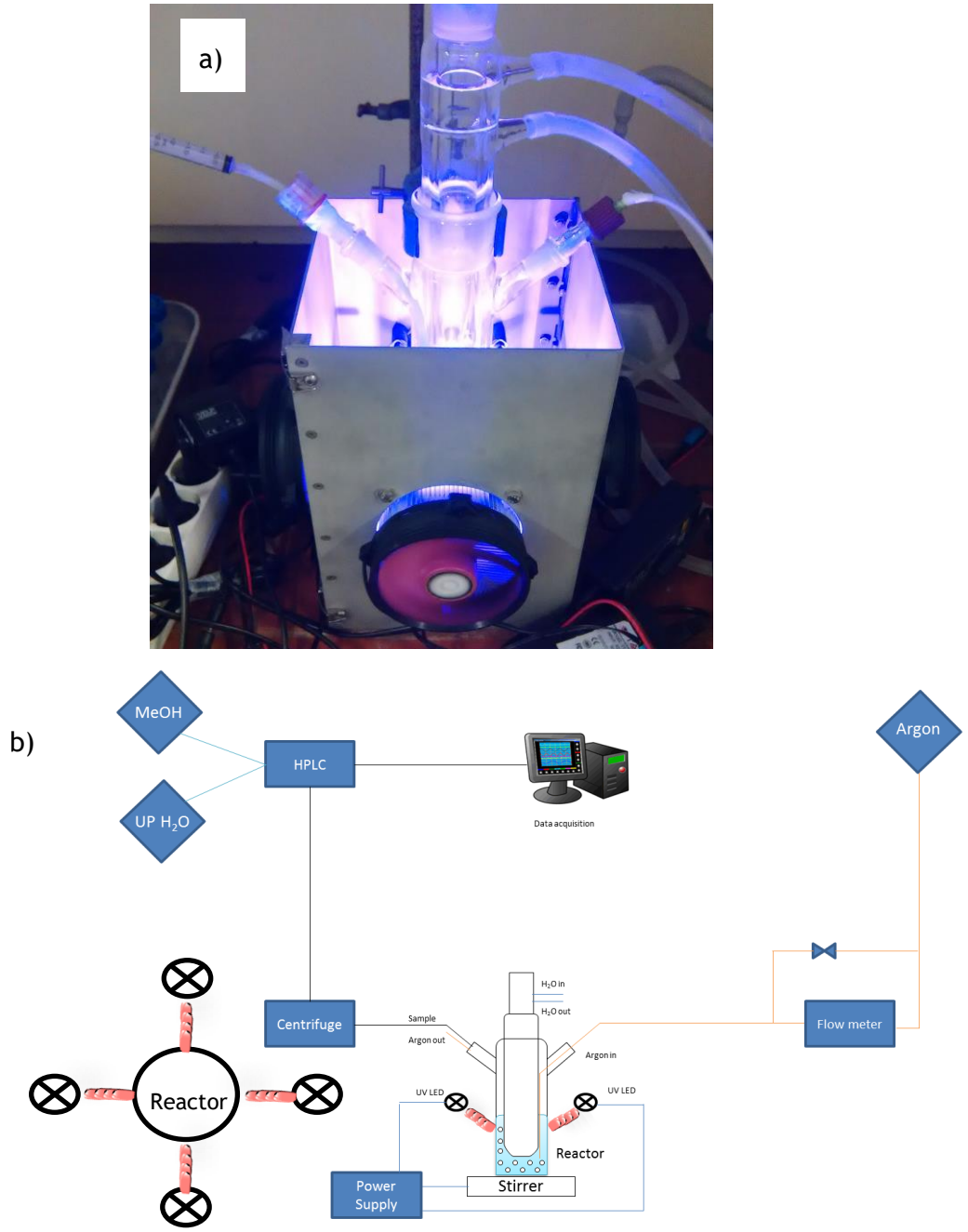


**Figure 8 -** Photocatalytic reaction setup: a) photograph whilst a reaction is happening; b) schematic representation, with view from the top of the photoreactor on the left.

Experiments utilizing a 1500 W xenon (Xe) lamp irradiating from the top, with the intent of simulating solar light were also made, using a Solarbox 1500e system (CO.FO.ME.GRA) using a cut-off soda-lime glass UV filter (for $\lambda < 290$ nm) with infrared reflection coating, to simulate outdoor exposure (irradiance equal to 30.9 mW $cm^{-2}$, determined with an Ocean Optics spectroradiometer in the range 300–650 nm) [84]. In this case, a cylindrical reactor similar to the one described by Sampaio et al. [85] was employed, the difference being the volume of the reactor (175 mL; dimensions: length: 6 cm; internal and external

diameteres of 4.5 cm and 5 cm, respectively), and the fact that the reactor was purged with Argon gas, as in the UV experiments. The volume of the reaction solution/suspension was kept at 100 mL.

The temperature was set so that the system would not surpass 40 ºC. There was no water reflux system, but only an air vent from the sides, to prevent over-heating. A photograph of the solar simulator equipment can be observed on Figure 9 a. Another picture was taken of the mounted system, as can be seen from Figure 9 b. A schematic representation of the described system is shown in Figure 9 c.

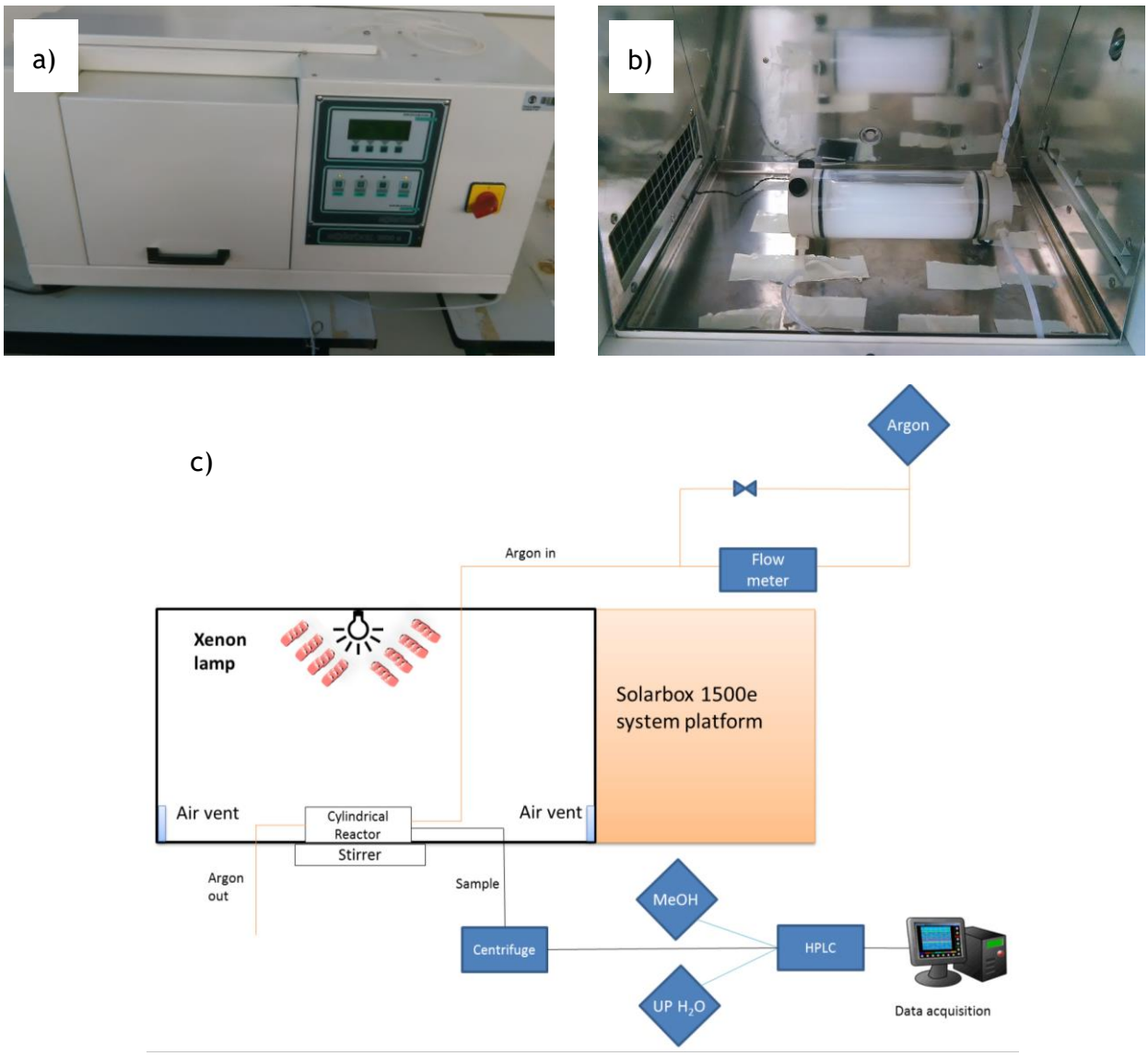


**Figure 9 -** Solar simulator setup: a) photograph of solar simulator; b) picture of the reactor; c) schematic representation of the reaction setup.

## 3.4 Analytical Methods

In this section is described the equipment and conditions used for product analysis and for catalysts' characaterization.

### 3.4.1 High Performance Liquid Chromatography (HPLC)

The concentration of BP and reaction products was determined by High Performance Liquid Chromatography (HPLC) with a Hitachi Elite LaChrom system equipped with a diode array detector (L-2450), a solvent delivery pump (L-2130) and a Lichrocart Purospher Star RP-18 endcapped column (250 mm x 4.6 mm, 5 μm particles), using a mobile phase consisting of a mixture water (A): methanol (B) in a gradient step. The method initiates using A:B (20:80) in a gradient step during 6 min for A:B (10:90), which was maintained for 9 min. After that, the mobile phase is changed to the initial proportion and allowed to stabilize during 4 min.

### 3.4.2 Diffuse reflectance UV-Vis (DRUV) spectroscopy

Diffuse Reflectance UV-Vis spectra (200-800 nm) of the powder samples were obtained with the Jasco V-560 UV-Vis spectrophotometer, with a double monochromator, double beam optical system. The equipment had an integrating sphere attachment (JASCO ISV-469), and the reflectance spectra were converted by the instrument software to equivalent absorption Kubelka-Munk. The UV-Vis spectra of BP, BH and BPC solutions were recorded in a JASCO V-560 UV–vis spectrophotometer.

### 3.4.3 Diffuse reflectance Infrared Fourier Transformed (DRIFT) spectroscopy

Fourier transform infrared (FTIR) measurements were performed on a FTIR JASCO 6800 equipped with a MIRacleTM Single Reflection ATR (attenuated total reflectance ZnSe crystal plate) accessory (PIKE Technologies, USA).

### 3.4.4 Transmission Electron Microscopy

Transmission electron microscopy (TEM) images were obtained using LEO 906E instrument operating at 120 kV, equipped with a 4 M pixel 28 × 28 mm CCD camera from TRS.

### 3.4.5 BET specific surface area

The surface area of the prepared materials was determined from the $N_2$ adsorption–desorption isotherms obtained at 77 K in a Quantachrome NOVA 4200e apparatus. The Brunauner–Emmett–Teller (BET) specific surface areas ($S_{BET}$) were calculated from nitrogen adsorption in the relative pressure range from 0.05 to 0.15.

# 4 Results and Discussion

One of the main objectives of this study is to assess the efficiency of the photocatalytic production of BH through BP reduction using different catalysts. Additionally, semiconductor's properties were examined and reaction assays performed, which are described in this chapter.

## 4.1 Catalysts' characterization

### 4.1.1 DRIFT and UV-Vis spectroscopic analysis

The FTIR-ATR spectra of bare and metal loaded $TiO_2$ P25 are shown in Figure 10 a, where the typical band of $TiO_2$ materials corresponding to Ti-O vibration can be observed peaking at c.a. 700 $cm^{-1}$ [86]. A broad band located between 2500 and 3800 $cm^{-1}$ attributed to the stretching vibrations of hydrogen bonded surface water molecules and hydroxyl groups can also be observed. The presence of some weak bands around 1620 and 1680 $cm^{-1}$ caused by bending vibration of coordinated water as well as from the Ti–OH group is also observed in all spectra [87]. The introduction of metal nanoparticles did not produce any important change in the FTIR spectrum of P25, which points out to the fact that no significant structural alteration is introduced in the metal oxide semiconductor by the addition of noble metals. In the case of $TiO_2$ SA, the bands corresponding to the Ti-OH groups are not evident as in the case of P25 (see Figure 10 b).

Taking shows the vibrational spectra of g-$C_3N_4$ and its precursor (dicyandiamide) of Figure 10 c, g-$C_3N_4$ spectrum exhibits a broad band located between 2700 and 3500 $cm^{-1}$ corresponding to the stretching O-H vibrations of adsorbed water and to N-H stretching vibration of primary and secondary amines [88]. The peaks located at 1625 and 1230 $cm^{-1}$ can be ascribed to C–N heterocycle stretches [89]. The bands appearing at 800-1700 $cm^{-1}$ are attributed to *s*-triazine derivatives [90]. N–H wagging bands can be observed in the range 910–700 $cm^{-1}$ [91]. The absence of bands at c.a. 2200 $cm^{-1}$ corresponding to C≡N, existent only in the dicyandiamide – DCM - spectrum, indicates complete polymerization during the thermal treatment.

The diffuse reflectance UV-Vis spectrum of photocatalysts provides important information about the optical and electronic properties of the materials. $TiO_2$ P25 and SA spectra reveals that these materials have a strong absorption in the UV range ($\lambda$<400 nm), while g-$C_3N_4$ has an absorption onset at c.a 500 nm (see Figure 10 d). The introduction of metal nanoparticles in P25 led to an increase in the absorption in the visible range, as well as a small augmented absorbance in the UV region, showing a broader absorbance than the P25 catalyst. For Au/P25 it is notorious the presence of a well-defined band peaking at 590 nm due to surface plasmon resonance (SPR) characteristic of Au nanoparticles [37, 43, 92-94].

The bandgap of these materials were determined from the respective Tauc plots (Figures 10 e and 10 f) and are summarized in Table 1.

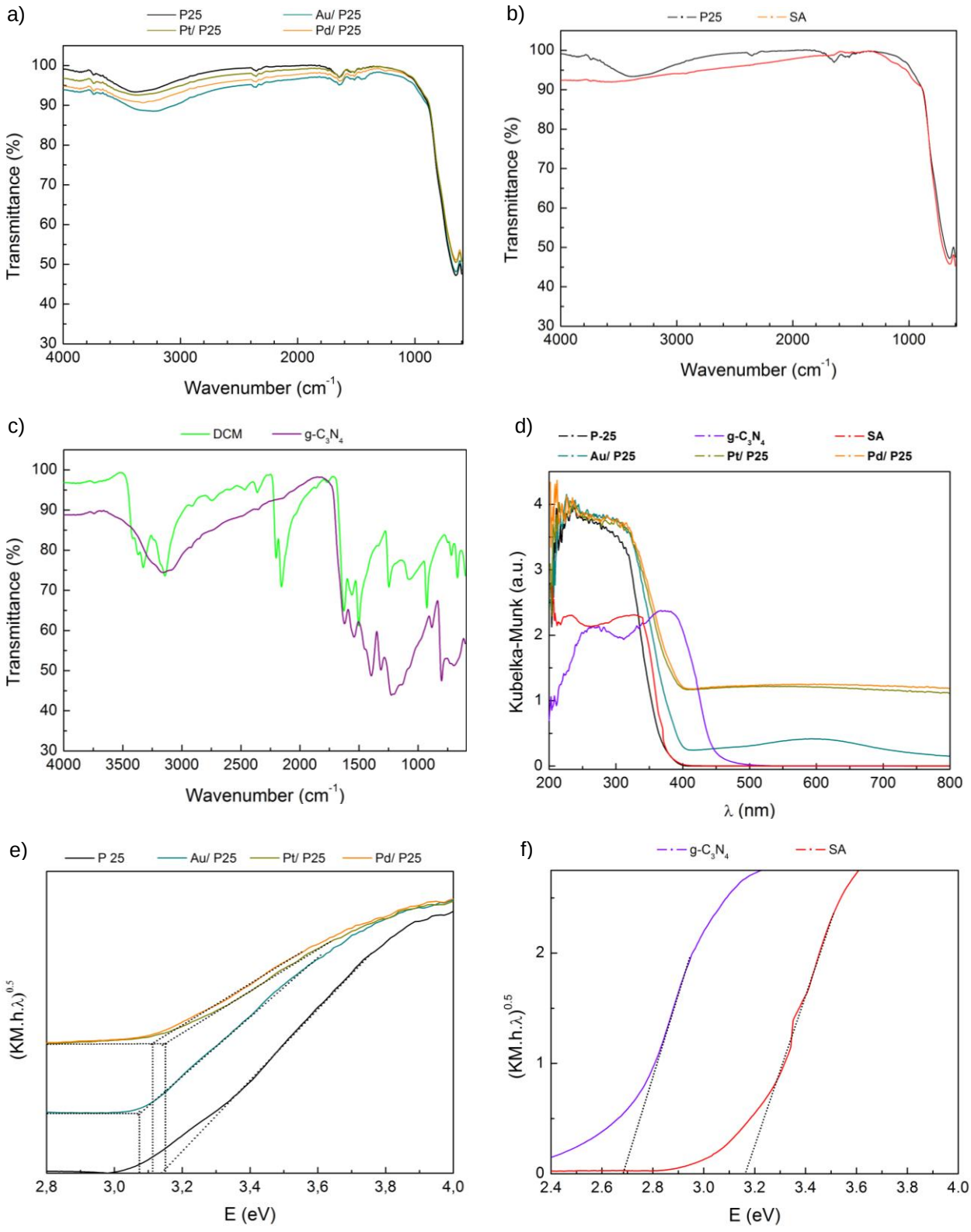


**Figure 10 -** ATR spectra of: a) bare and metal-loaded $TiO_2$ P25; b) $TiO_2$ P25 and $TiO_2$ SA; c) DCM and g-$C_3N_4$. DR UV-Vis spectra of different catalysts: d) bare and metal-loaded $TiO_2$ P25, $TiO_2$ SA and g-$C_3N_4$. Tauc plots of: e) bare and metal-loaded$TiO_2$ P25; f) $TiO_2$ SA and g-$C_3N_4$.

Similar bandgap values were obtained for $TiO_2$ P25 and SA. On the other hand, g-$C_3N_4$ has a band gap of c.a. 2.7 eV, which means that a less energetic radiation is needed to excite this material, and also that it can be probably active under visible light conditions [95].

Surprisingly, $TiO_2$ P25 and Pt/P25 have relatively the same band gap, at about 3.15 eV, while Pd/P25 has 3.11 eV. The observed band gaps of Pt and Pd modified P25 are too large to harness visible light and consequently, these catalysts should not show increased activity under visible illumination when compared to UV conditions. However, changes on radiation wavelength absorption should not affect on photocatalytic activity, since this depends on recombination rate, among other factors [96]. Due to the fact that the cocatalysts show more absorbance in the UV region than the $TiO_2$ P25, better photocatalysts could have been fabricated, although Pt/P25 and Pd/P25 may not to be visible light active.

Loading with Pt and Pd did not affect significantly the bandgap of the resulting $TiO_2$ P25 based materials. A decrease in the bangap from 3.15 to 3.01 eV was obtained for Au/P25, which may be attributed to the band shrinkage effect as a result of the gold nanoparticles deposition on the support surface [37, 97].

### 4.1.2 Transmission electron microscopy and BET surface area

Figure 11 shows typical TEM micrographs of $TiO_2$ P25 loaded with different metal nanoparticles. It can be observed that P25 is constituted by spheroidal nanoparticles of c.a. 30-50 nm aggregated as larger particles.

The presence of metal nanoparticles (darker spots, see arrows) could be observed, which were well dispersed in P25. The metal particle size distributions were evaluated by measuring metal particle diameters in TEM images (see Table 1). The dimensions of the metal nanoparticles loaded on P25 were of the order of magnitude of 21±2 nm.

$TiO_2$ SA is constituted by crystals of larger dimensions than $TiO_2$ P25 (Figure 11 d), with sizes of hundreds of nanometers. Finally, g-$C_3N_4$ shows a layered morphology as depicted in Figure 11e.

**Table 1 -** Average particle size, mode, particle size range, surface area ($S_{BET}$) and band gap of $TiO_2$ derived catalysts and g-$C_3N_4$.

| Catalyst | Impregnated Metal | $S_{BET}$ ($m^2 g^{-1}$) | Average metal particle size (nm) | Mode (nm) | Metal particle size range (nm) | Bandgap (eV) |
|---|---|---|---|---|---|---|
| $TiO_2$ P25 | - | 56 | - | - | - | 3.15 |
| | Au | - | 19.4 | 20-25 | 8-30 | 3.08 |
| | Pd | - | 23.1 | 20-25 | 8-30 | 3.11 |
| | Pt | - | 22.4 | 20-25 | 6-30 | 3.16 |
| $TiO_2$ SA | - | 13 | 150.2 | 185-190 | 78-250 | 3.15 |
| g-$C_3N_4$ | - | 9 | - | - | - | 2.69 |

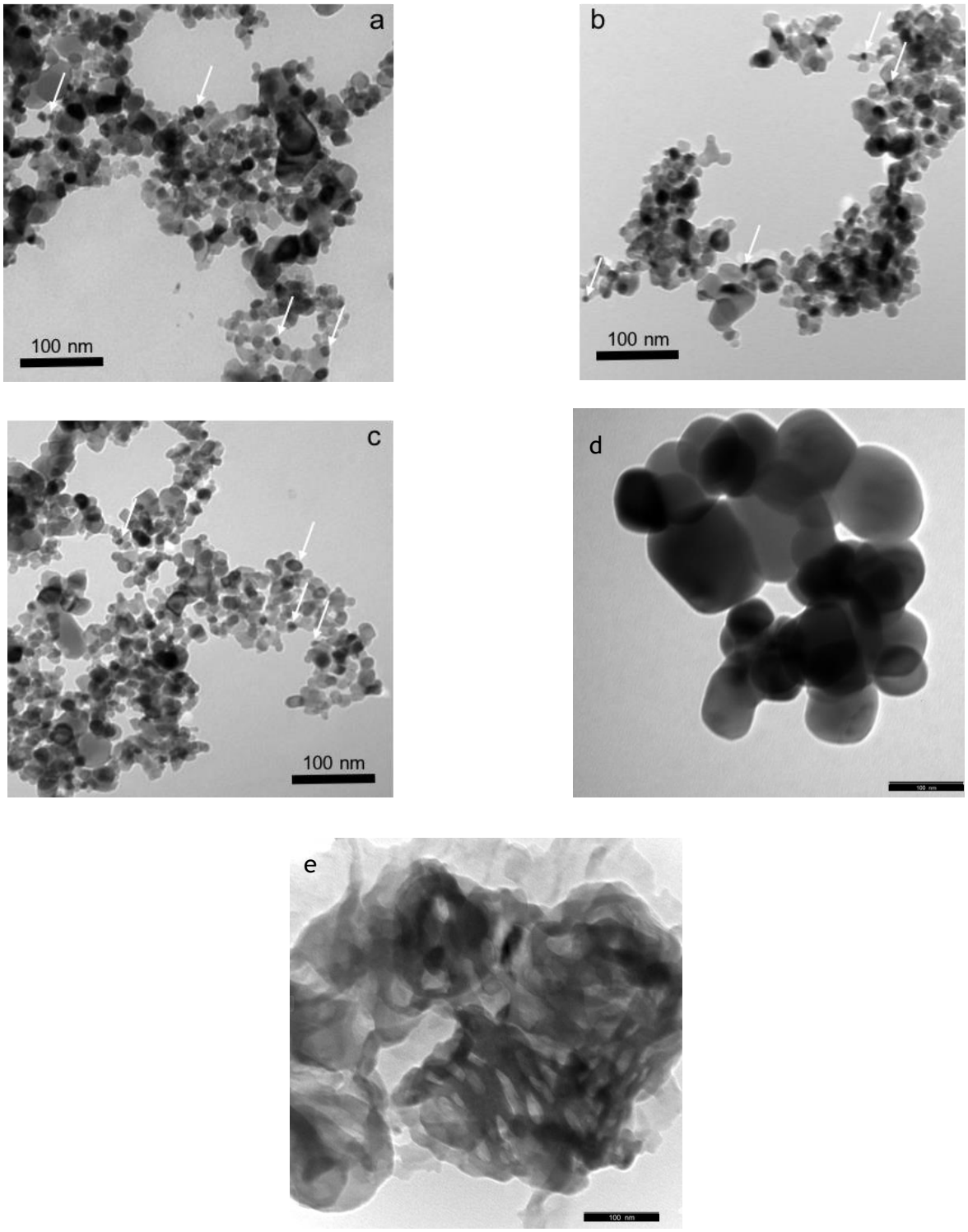


**Figure 11 -** TEM images of: a) Pd/P25; b) Au/P25; c) Pt/P25 (with arrows are pointing to some examples of metal nanoparticles); d) $TiO_2$ SA and e) g-$C_3N_4$.

BET surface area of selected materials is also available from Table 1. The highest $S_{BET}$ (56 $m^2\,g^{-1}$) was observed for $TiO_2$ P25. The surface area of the metal-loaded materials was not determined but it is not expected to vary too much in relation to $TiO_2$ P25, since a very low amount of metal was used. $TiO_2$ SA and g-$C_3N_4$ show lower surface areas of 13 and 9 $m^2\,g^{-1}$, respectively.

## 4.2 Photoinitiated reactions

This section of the work will be showing and discussing the results on the topic of the photoinitiated reactions performed. The first sample was taken in order to have an initial solution concentration value, ensure that the reaction did not occur in the dark and to assess the possibility of BP adsorption on the catalyst.

Kinetic study was not approached over the course of this work since these are quite complex and need a significant amount of experiments to be determined [13, 14].

The efficiency of the photo-assisted production of BH from BP was evaluated taking into consideration the initial reaction rate of BP abatement ($r_{i,BP}$), and the initial reaction rate of BH formation ($r_{i,BH}$), calculated by the slope of the tangent to the initial points of the concentration versus time plot. In this case, since few points were taken in the first instants of the reactions, the initial reaction rates were calculated as follows:

$$r_{\mathrm{i,BP}} = -\frac{[\mathrm{BP}]_{5\ \mathrm{min}} - [\mathrm{BP}]_{0\ \mathrm{min}}}{5-0} \quad (5)$$

$$r_{\mathrm{i,BH}} = \frac{[\mathrm{BH}]_{5\ \mathrm{min}} - [\mathrm{BH}]_{0\ \mathrm{min}}}{5-0} \quad (6)$$

BP conversion, and BH selectivity and yield were determined at 10 minutes, since in most cases at this reaction time there is a significant fraction of BP converted into BH. These parameters were determined usin the following equations:

$$\mathrm{C} = 1 - \frac{[\mathrm{BP}]_{10\ \mathrm{min}}}{[\mathrm{BP}]_{0\ \mathrm{min}}} \quad (7)$$

$$\mathrm{S} = \frac{[\mathrm{BH}]_{10\ \mathrm{min}} - [\mathrm{BH}]_{0\ \mathrm{min}}}{[\mathrm{BP}]_{0\ \mathrm{min}} - [\mathrm{BP}]_{10\ \mathrm{min}}} \quad (8)$$

$$\mathrm{Y} = \frac{[\mathrm{BH}]_{10\ \mathrm{min}} - [\mathrm{BH}]_{0\ \mathrm{min}}}{[\mathrm{BP}]_{0\ \mathrm{min}}} \quad (9)$$

Typical experiments were performed using a molar concentration of BP of 1.5 mM.

The first set of experiments where performed using iPrOH as solvent, since it allows BP to easily dissolve, allows the good suspension of the catalyst particles and prevents fast recombination of the semiconductor, since it acts as hole scavenger [77]. A great amount of other hole scavengers have been reported to give good yields of product [45-47, 98], but polar solvents are preferred for the abstraction of hydrogen [99]. The photoreduction of BP was studied using other alcoholic solvents over the course of this work, which have also been successfully used in other photocatalytic reactions as reported in [23].

It is generally accepted that the limiting step for the photochemical reduction of BP, while using alcohols as solvents, is the abstraction of hydrogen atoms from the alcohol [18]. Meanwhile, small amounts of salts have proven to selectively reduce BP to BH, such as sodium alcoholate on ethanol [6], and aldehydes into their corresponding products, with sodium hydroxide, also on an ethanolic solution [77]. Other studies were made with KOH for photoreductions, and it was proven that this salt enances the abstraction of a hydrogen atom from iPrOH, the proton donor used for this work [55, 56, 100-103]. Therefore, a 0.1 M KOH solution in iPrOH was prepared and introduced in small quantities in the reaction

environment. As shall be reviewed later in this study, the presence of KOH is crucial to the selective production of BH from BP.

Some of the studies made include the effect of catalyst load, substrate (BP) concentration, presence and concentration of KOH, irradiance and type of solvent/hole scavenger, which were found to be crucial parameters in heterogeneous photocatalytic reactions [104].

### 4.2.1 Photochemical versus Photocatalytic production of BH from BP

The conversion of BP into BH was studied in the absence and in the presence of $TiO_2$ P25 as catalyst for comparing the photochemical and the photocatalytic routes. Photocatalytic reactions were carried out using a $TiO_2$ P25 load of 1 g $L^{-1}$. In this series of reactions, a molar concentration of 10 mM of KOH was applied. Assays in the absence of radiation with and without catalyst were also performed to ensure that the reaction is photoinitiated only. The results of these reactions are presented in Figure 12. At first glance from Figure 12 a, it is confirmed that BP conversion does not happen in the dark, whether in the presence or absence of catalyst. It correspondingly proves that the BP adsorption is irrelevant and that no BP conversion occurs in the dark.

As can be observed in Figure 12 a, the initial rate of the photocatalytic conversion of BP is higher than for the photochemical reaction. Nevertheless, at the end of 60 min of reaction, a higher conversion of BP could be achieved throughout the photochemical route. Moreover, there seems to be an increase in the amount of BH formed under photocatalytic conditions, comparing to the photochemical process (Figure 12 b). Overall, an increase in conversion and selectivity of close to 10% is observable and provides an advantage in operating with a photocatalytic reaction. Worth noting is the initial tendency for the photochemical reaction, which seems to have an induction period. This may be due to the complexity of the photochemical mechanism. Table 2 summarizes the initial reaction rates for both photochemical and photocatalytic experiments.

Observing Table 2, the initial velocity for the photocatalytic reaction is quite superior to the photochemical reaction, both for the conversion of BP and for the production of the compound of interest. The presence of catalyst led to an increase in the efficiency of BH production, enhancing the yield and selectively, by shifting the reaction toward the hydrogenation of BP.

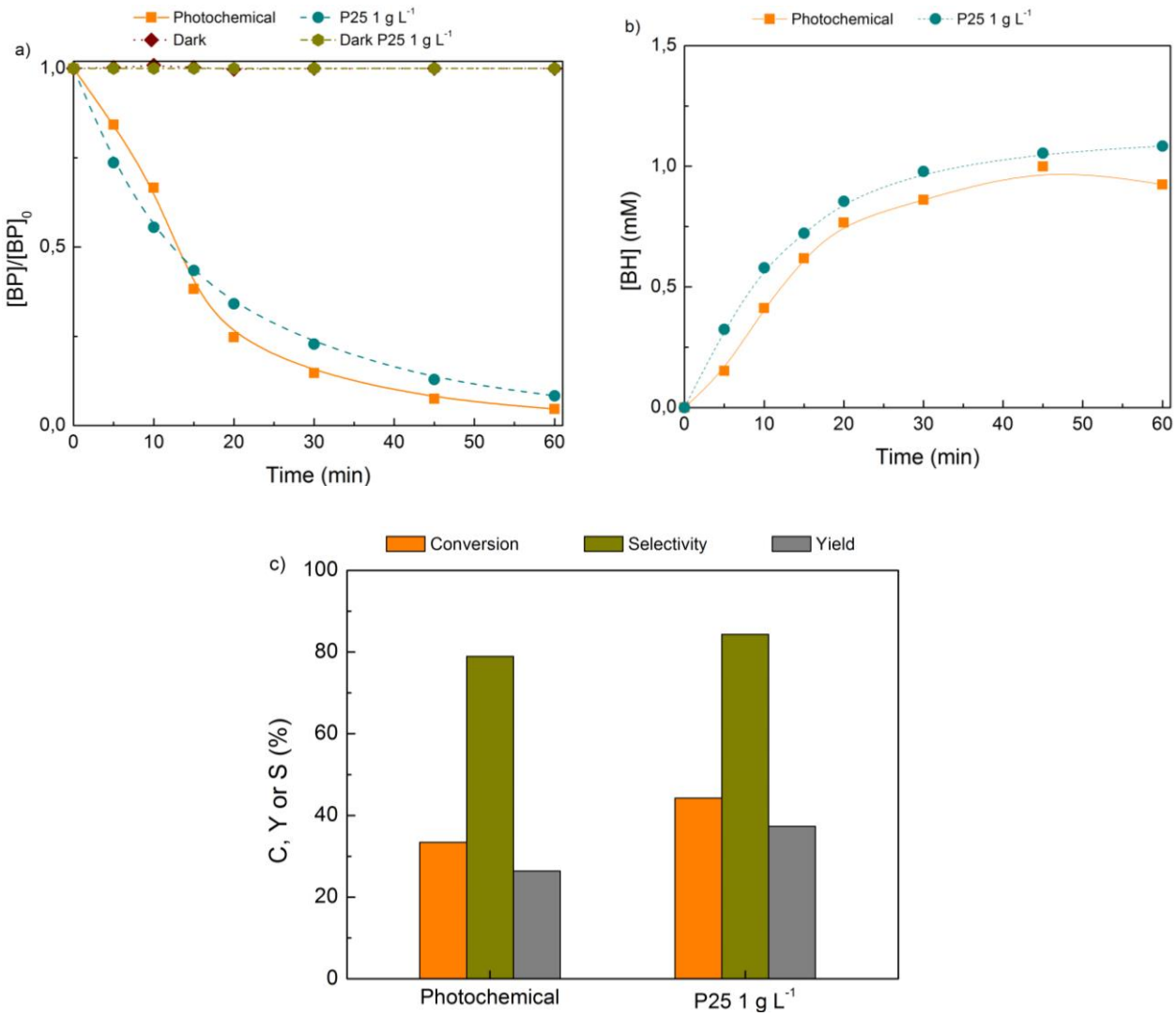


**Figure 12 -** Photochemical and photocatalytic production of BH from BP; $[BP]_0$=1.5mM; [KOH]=10 mM; solvent: isopropanol: a) Normalized BP concentration profiles during the reaction; b) BH concentration profiles during the reaction; c) BP conversion, yield and selectivity toward BH formation at 10 min of reaction.

**Table 2 -** Initial reaction rates for the reduction of BP ($r_{i,BP}$) and BH formation ($r_{i,BH}$) for the photochemical and photocatalytic reactions, with [KOH]=10 mM.

| **Reactions** | $r_{i,BP}$ **x 10$^2$ (mM min$^{-1}$)** | $r_{i,BH}$ **x 10$^2$ (mM min$^{-1}$)** |
|---|---|---|
| Photochemical | 4.7 | 3.0 |
| Photocatalytic | 8.1 | 6.5 |

Reactions in the absence of KOH were also performed, with the remaining conditions being kept constant, in order to observe whether the salt's presence is of advantage or not. The results are presented in Figure 13.

It was observed that the photochemical degradation of BP is quite rapid, quite faster than the photocatalytic reaction (Figure 13 a). The initial tendency is also different from the one shown in Figure 12 a, where the photocatalytic degradation was superior to the one in the absence of catalyst. This may mean that under these conditions, the catalyst may actually be delaying the degradation phase of the reaction, probably through a different mechanism, as proposed before. It may also be that the solid is in excess for this reaction (since catalyst load was not yet optimized at this point), not allowing for proper photon absorption. The formation of BH followed the same tendency, i.e. the photochemical reaction induces a rapid raise in the amount of BH in the first moments, while for the photocatalytic reaction, this increase in BH concentration is more gradual (Figure 13 b). According to Escobar et al. [23], when the photoreduction of a ketone is given under the presence of a semiconductor, the compound distribution changes to the corresponding alcohol, instead of other products, that come from the addition or dimerization of intermediate species. In the absence of KOH, BPC is detected as the main reaction product, while the amount of this undesired species is lower for the photocatalytic reaction (Figure 13 c). Thus, although BP conversion appears lower for the photocatalytic process, the selectivity toward BH formation was higher, which confirms the advantage of using photocatalysis for BH production (Figure 13 d). The reaction rates listed in Table 3 are in agreement with the previous conclusions.

Almost all the parameters were different when comparing the reactions with and without the catalyst. The presence of the photocatalyst affects the reaction in a positive way, when intending to produce BH and avoiding high yields of BPC. However, a faster rate of BP conversion for the photochemical reaction was attained, observing Table 3. The obtained results suggest that different reaction mechanisms should be involved. Additionally, the initial rates for product formation are quite similar for these last two assays and relatively low when compared to the previous series of experiments (in the presence of KOH) given on Table 2. In the absence of KOH, BP hydrogenation is quite slow through both photochemical and photocatalytic reactions and substancial ammounts of BPC are formed. Although the presence of KOH leads to a decrease of BP conversion rate, the selectivity and rate of formation for the desired product is increased, due to its ability of facilitating hydrogen extraction from isopropanol. For this work, it was found that the photocatalytic reaction is indeed an improvement over the photochemical reaction, especially under the presence of KOH.

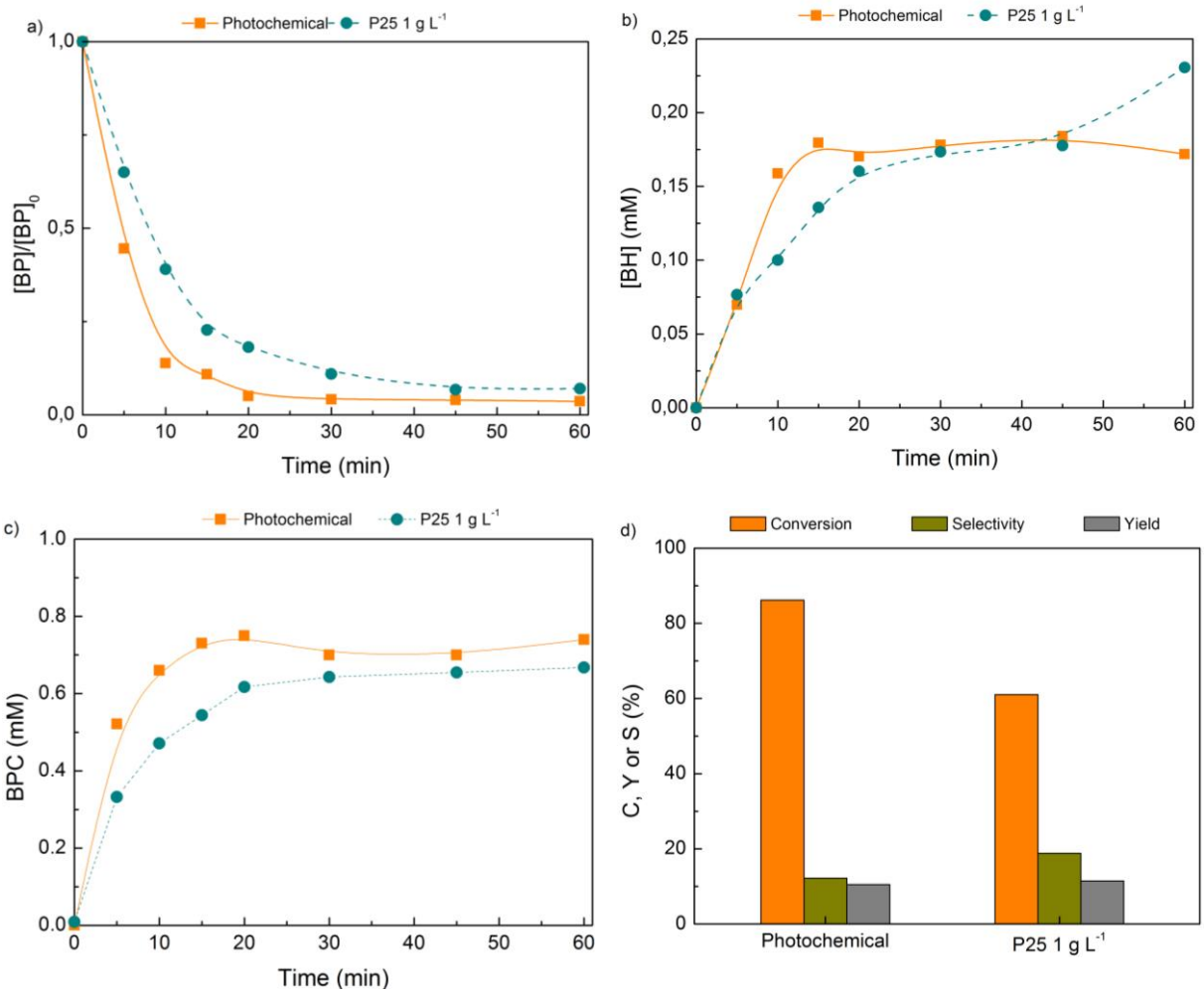


**Figure 13 -** Photochemical and photocatalytic production of BH from BP in the absence of KOH; $[BP]_0$=1.5 mM; solvent: isopropanol: a) Normalized BP concentration profiles during the photochemical and photocatalytic reactions; b) BH concentration profiles during the reactions; c) BPC concentration profiles; d) BP conversion, yield and selectivity toward BH formation at 10 min of reaction.

**Table 3 -** Initial reaction rates for the reduction of BP ($r_{i,BP}$) and BH formation ($r_{i,BH}$) for the photochemical and photocatalytic reactions in the absence of KOH.

| **Reactions** | $r_{i,BP}$ **x 10$^2$ (mM min$^{-1}$)** | $r_{i,BH}$ **x 10$^2$ (mM min$^{-1}$)** |
|---|---|---|
| Photochemical | 16.8 | 1.4 |
| Photocatalytic | 10.5 | 1.5 |

### 4.2.2 Effect of $TiO_2$ P25 load

In order to avoid an ineffective excess of catalyst and to ensure a total absorption of efficient photons, the optimum mass of catalyst used in the photocatalytic reactions needs to be found [39]. It is also known that the rate of photocatalytic reactions is highly dependent of the catalyst load [85]. A rate that increases proportionally with catalyst load shows a true heterogeneous catalytic regime. But over a certain catalyst

quantity in solution, the reaction rate drops. This limit corresponds to the maximum amount of catalyst at which all particles are totally illuminated and depends on the geometry and on the working conditions of the photoreactor. An extra addition of catalyst will not produce effective results. Furthermore, excessive catalyst charge may produce a screening effect resulting in a decrease in the efficiency of the process.

The catalyst load used in the preliminary photocatalys studies (1 g $L^{-1}$) was chosen based in reports in which this was found as the optimal $TiO_2$ P25 load [39, 105, 106]. An increase in the catalyst load to 1.25 g $L^{-1}$ did not produce any significant effect in the reaction efficiency (Figures 14 a-c). Presumibly, the solid is in excess on the reactional environment. So, the catalyst load was lowered and new experiments were carried out, ranging $TiO_2$ load from 0.25 to 0.05 g $L^{-1}$. An increase in BP conversion and BH production was observed when increasing the catalyst load from 0.05 g $L^{-1}$ to 0.1 g $L^{-1}$. A further increase in the catalyst load appeared to be detrimental for the efficiency of the process.

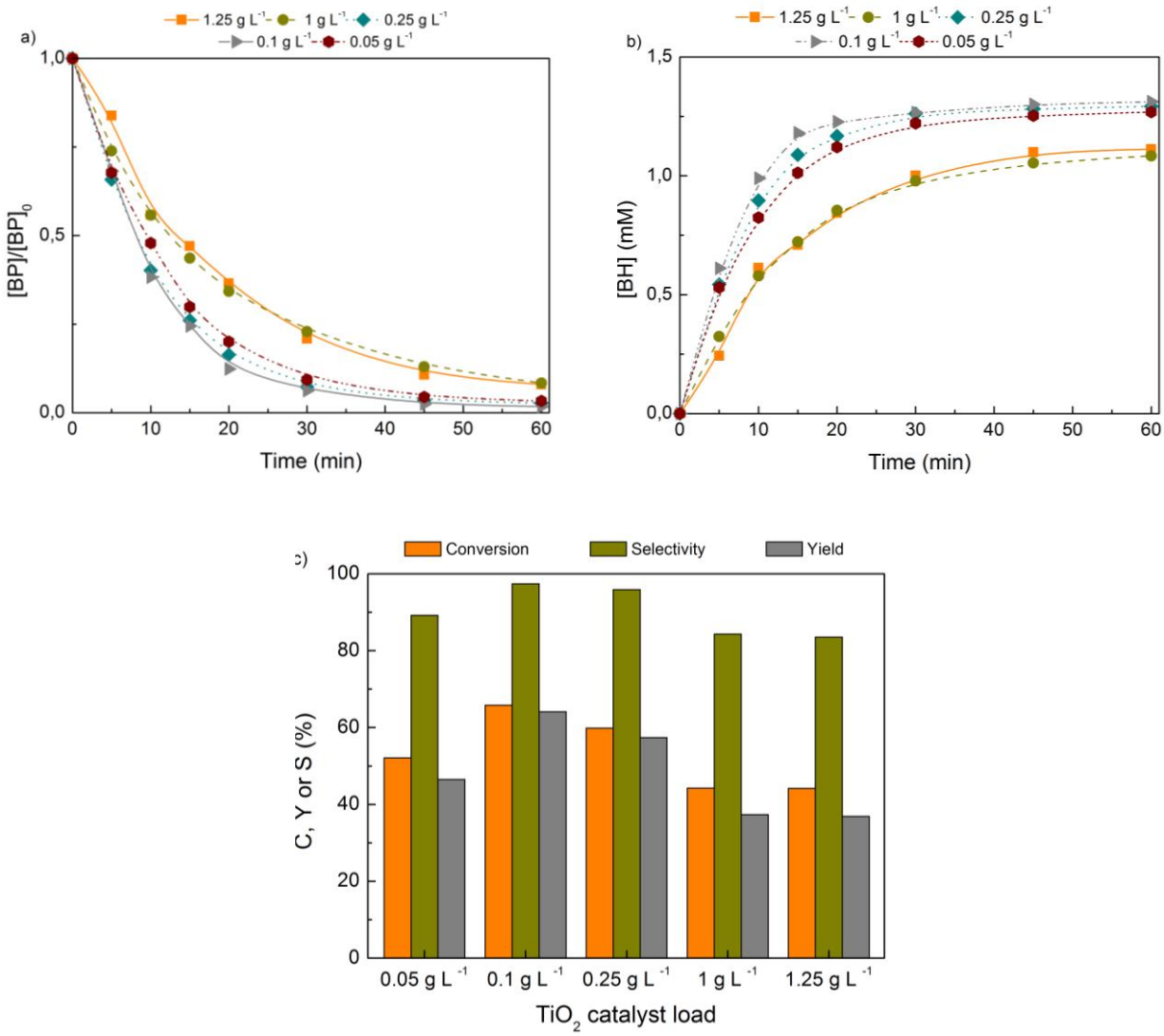


**Figure 14 -** Effect of $TiO_2$ P25 load in photocatalytic production of BH from BP; $[BP]_0$=1.5 mM; [KOH]=10 mM; solvent: isopropanol: a) Normalized BP concentration profiles during the photocatalytic reduction of BP; b) BH concentration profiles during the photocatalytic reactions; c) BP conversion, yield and selectivity toward BH formation at 10 min of reaction.

For the formation of BH, a maximum amount was achieved at a $TiO_2$ load of 0.1 g $L^{-1}$. The same tendency was observed for the conversion, selectivity and yield (Figure 14 c). The peak selectivity was of 97%.

Initial reaction rates are presented on Table 4.

**Table 4 –** Effect of $TiO_2$ P25 load on the initial rates for the reduction of BP ($r_{i,BP}$) and BH formation ($r_{i,BH}$) .

| **P25 Catalyst load Reactions (g $L^{-1}$)** | $r_{i,BP}$ **x $10^2$ (mM $min^{-1}$)** | $r_{i,BH}$ **x $10^2$ (mM $min^{-1}$)** |
|---|---|---|
| 1.25 | 5.0 | 4.1 |
| 1 | 8.1 | 6.5 |
| 0.25 | 10.5 | 10.2 |
| 0.1 | 10.9 | 10.7 |
| 0.05 | 9.4 | 7.7 |

The top rate for the formation of BH and BP degradation is also at 0.1 g $L^{-1}$, being this considered the optimal catalyst load achieved, using the conditions: iPrOH as solvent and [KOH]=10 mM.

### 4.2.3 Effect of KOH concentration

As analyzed beforehand, an increase in the efficiency of the photoinitiated reaction is observed when KOH is added to the reactiom medium. It has been reported that the presence of KOH induces hydrogen abstraction from alcohols [107] and has been used in photoreduction reactions using several catalysts such as gold nanoparticles, ruthenium based catalysts and supported noble metal nanoparticles [55, 56, 100-103].

A study on the effect of KOH concentration in the efficiency of the photocatalytic process was also performed. In order to guarantee the accomplishment of the goal for this project, there is a need to reduce the amount of this compound, but without compromising the production of BH. Therefore, a study of this salt concentration ranging from 10 to 1 mM was performed. The results are presented in Figure 15.

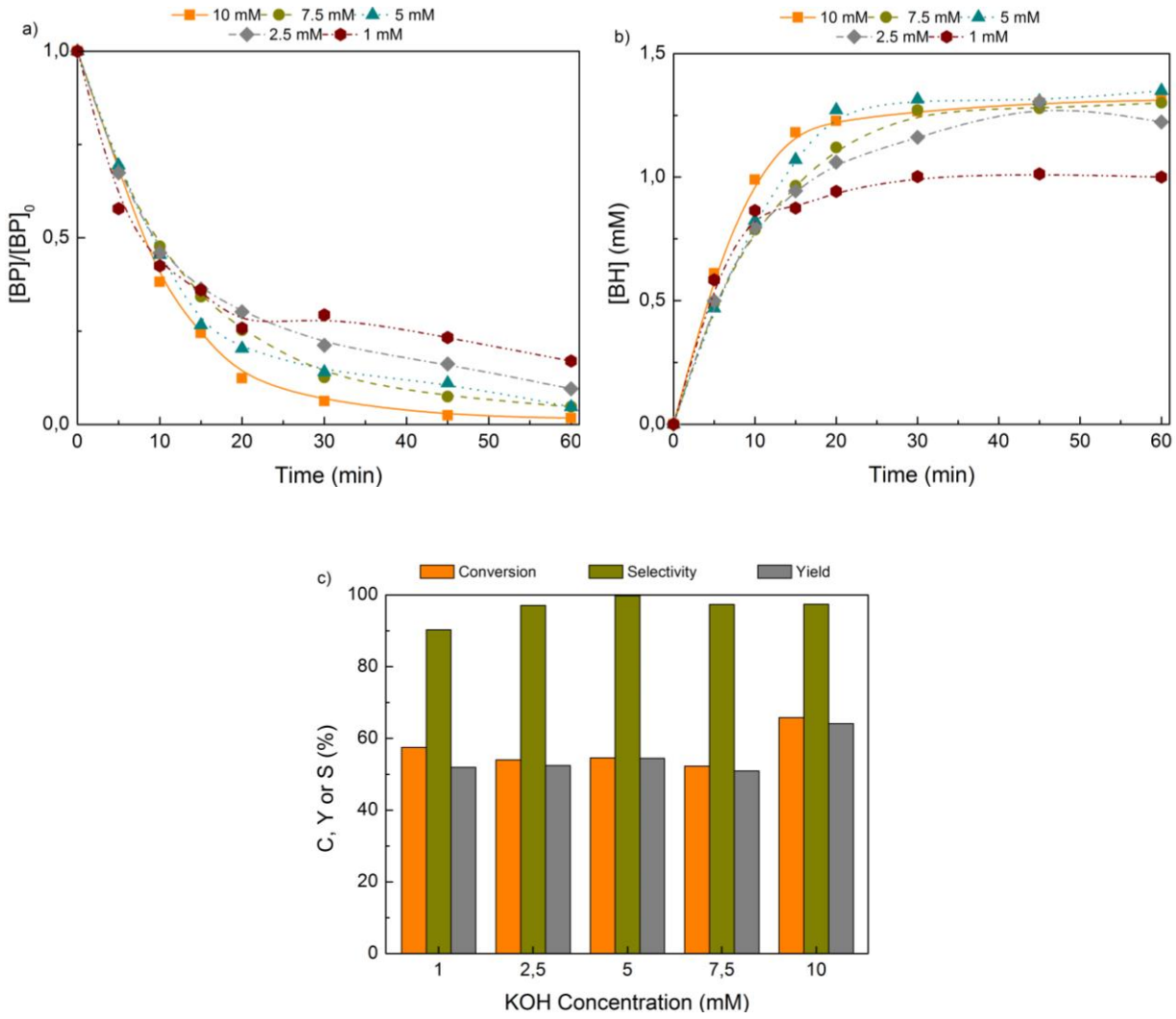


**Figure 15 -** Effect of KOH concentration on photocatalytic reduction of BP; $[BP]_0$=1.5mM; $TiO_2$ P25 load = 0.1 g $L^{-1}$; solvent: isopropanol: a) Normalized BP concentration profiles during the photocatalytic reduction of BP; b) BH concentration profiles during the photocatalytic reactions; c) BP conversion, yield and selectivity toward BH formation at 10 min of reaction.

From Figure 15 a, a tendency for elevated concentrations inducing higher substrate decomposition is shown, especially toward the final reaction moments. In Figure 15 b it is possible to observe the same tendency for the first few minutes of reaction (up to 10 min), and then the amount of BH produced using 5 mM is slightly increased. Besides this, from Figure 15 c, the top selectivity is reached for this same concentration, although the others are not so far behind. Also, the lowest concentration shows a great initial production of BH, and good conversion. Pross et al. [77] reported results using sodium hydroxide - which is a similar base – on an alcoholic solution with $TiO_2$ catalyst as well, stating that hydroxide anions adsorb on the semiconductor surface, and that an excess of these negatively charged particles remains in suspension and causes a shortage of protons, slowing down the photoreduction reaction.

Though it is not shown in Figure 15, the reaction with the lowest amount of KOH exhibited the formation of BPC in measurable quantities, of about 0.1 mM after 60 minutes.

The conversion and yield are all quite similar, with only the highest concentration of KOH resulting in an increase of about 10% comparing with the other reactions. However, for the total reaction time, the maximum product formation is attributed to the 5 mM concentration.

Table 5 shows the initial reaction rates for this series of reactions.

**Table 5 -** Effect of KOH concentration in the initial rates for the reduction of BP ($r_{i,BP}$) and BH formation ($r_{i,BH}$) using a $TiO_2$ P25 load of 0.1 g $L^{-1}$.

| KOH concentration (mM) | $r_{i,BP}$ x $10^2$ (mM $min^{-1}$) | $r_{i,BH}$ x $10^2$ (mM $min^{-1}$) |
|---|---|---|
| 10 | 10.9 | 10.7 |
| 7.5 | 9.8 | 9.5 |
| 5 | 9.1 | 9.1 |
| 2.5 | 9.7 | 9.6 |
| 1 | 12.9 | 10.2 |

As mentioned before, the initial reaction rates for BP reduction and BH production are quite similar, although the reaction using the lowest KOH concentration (1 mM) show initial reacton rates slightly higher. However, looking at the whole reaction time, a lower amount of desired product is formed using the lowest KOH concentration and BPC also formed, decreasing selectivity.

For the reactions with greater amounts of KOH, a rising on both initial rates is also verified. Additionally, looking at the entire reaction time, and keeping in mind the objective of producing BH from BP while avoiding excessive caustic agent concentrations, a concentration of 5 mM was selected as the concentration for the following reactions. A concentration of 2.5 mM could also be a good option, from the green chemistry point of view, since it has very close performance to the 5 mM, whilst no undesired products are formed. However, further optimization should be made for this parameter, between the values of 5 and 1 mM. For this work performed, BPC was never formed under over 1 mM KOH concentrations.

### 4.2.4 Effect of initial concentration of BP

Initial concentration of substrate, ranging from 0.5 to 1.75 mM was also studied. The results are presented in Figure 16.

It was observed an increase in the initial rate of BP reduction as the initial BP concentration rises (Figure 16 a and Table 6). For the lowest initial BP concentration it seems to exist an induction time during the initial reaction period. This behavior has also been reported by Escobar et al. [23], which addressed the highest reaction rates found for higher BP initial concentrations due to competition between the

photocatalytic and the photochemical reaction, favored at high concentrations of BP and the photocatalytic reaction, which is predominant at low concentrations. The same tendencies are observed for Figure 16 b, where the similar bump is observable for the lowest concentration, and then BH production increases with initial concentration.

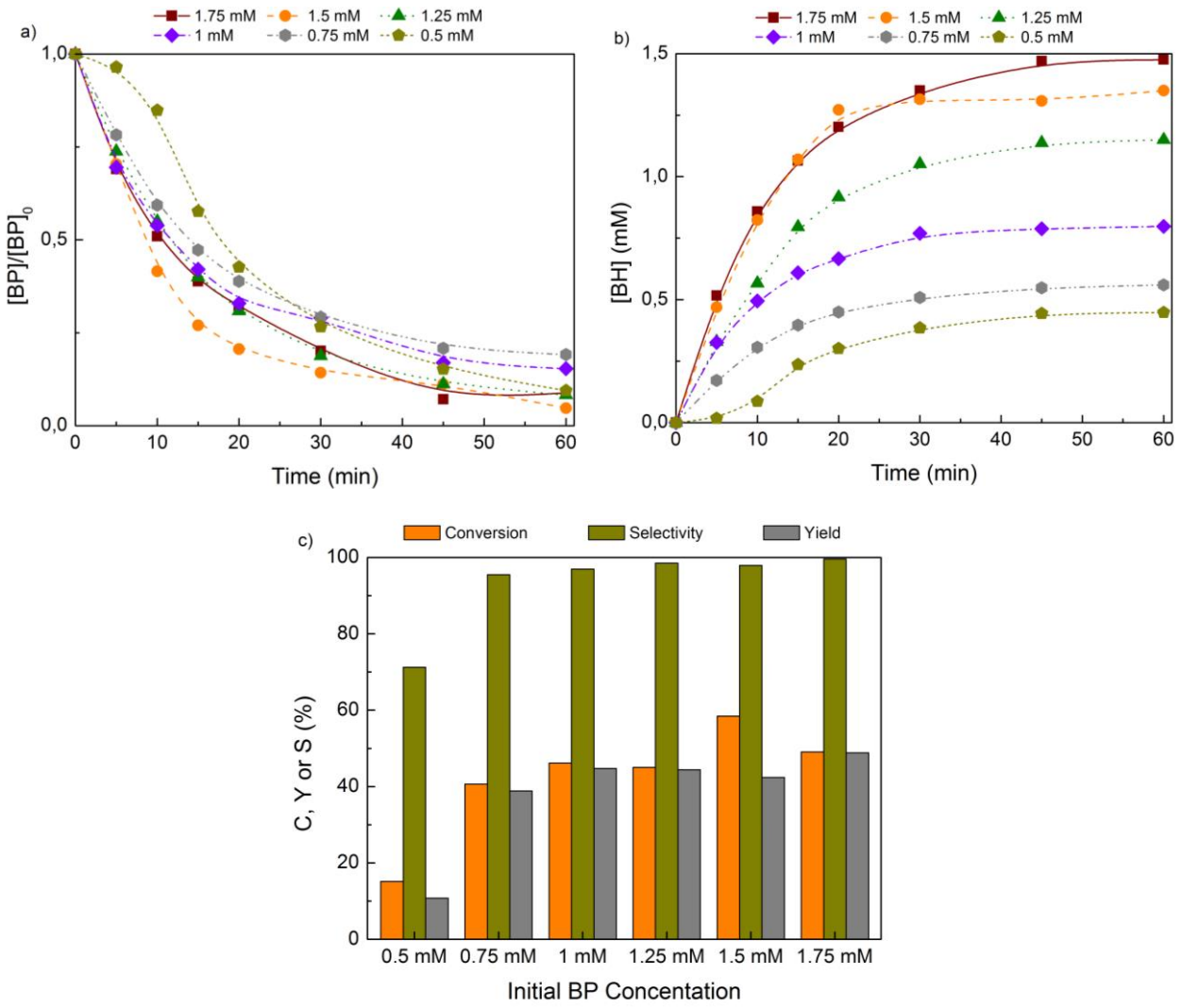


**Figure 16 -** Effect of the initial concentration of BP on the photocatalytic reduction of BP; [KOH]=5 mM; $TiO_2$ P25 load = 0.1 g $L^{-1}$; solvent: isopropanol: a) Normalized BP concentration profiles during the photocatalytic reduction of BP; b) BH concentration profiles during the photocatalytic reactions; c) BP conversion, yield and selectivity toward BH formation at 10 min of reaction.

Figure 16 c shows that selectivity rises with initial BP concentration, as well as the yield. Conversion is maximized for the reaction using 1.5 mM of substrate, which may point that it is the concentration at which the photocatalytic system has its highest efficiency at converting BP.

Table 6 summarizes the initial reaction rates over the course of changing initial concentrations of the substrate.

**Table 6 –** Effect of initial BP concentration of the initial rates of BP reduction ($r_{i,BP}$) and BH formation ($r_{i,BH}$), using [KOH] = 5 mM and a $TiO_2$ P25 load of 0.1 g $L^{-1}$.

| Initial BP concentration (mM) | $r_{i,BP}$ x $10^2$ (mM $min^{-1}$) | $r_{i,BH}$ x $10^2$ (mM $min^{-1}$) |
|---|---|---|
| 1.75 | 10.9 | 10.3 |
| 1.5 | 9.1 | 9.1 |
| 1.25 | 6.6 | 6.5 |
| 1 | 6.3 | 5.9 |
| 0.75 | 3.4 | 3.4 |
| 0.5 | 0.4 | 0.3 |

As expected, initial reaction rates increase with the amount of initial ketone existent in solution. At the lowest concentration, the value is quite inferior, due to the induction period observed at the start of the reaction.

### 4.2.5 Effect of UV light Irradiance

Experiments on the effect that the amount of energy irradiated by the UV LEDs has on the photocatalytic reactions where also performed. This study was performed by varying the amount of LEDs used for irradiating the reaction system: 4 LEDs or only 2 LEDs on, corresponding to a total irradiance of 2455 and 1230 W $m^{-2}$, respectively. The results are presented in Figure 17.

From Figure 17 a, it was observed an induction period for BP conversion for the reaction under the lowest irradiance. Similarlly in Figure 17 b, for the production of BH, the same effect is observed. Moreover, under these conditions, selectivity is lowered by about 5%, while conversion and yield were significantly affected (Figure 17 c).

Table 7 shows the initial rates for the reaction using different UV light conditions. The initial rates are very dissimilar, being much higher for the reaction under the highest irradiance (over 15 times superior). This should happen because in the first instants of the reaction using the 2-LED system there is insufficient photons to efficienctly activate the catalyst and promote the photocayalytic reaction. It can be concluded that the rate of reaction is proportional to the LEDs intensity.

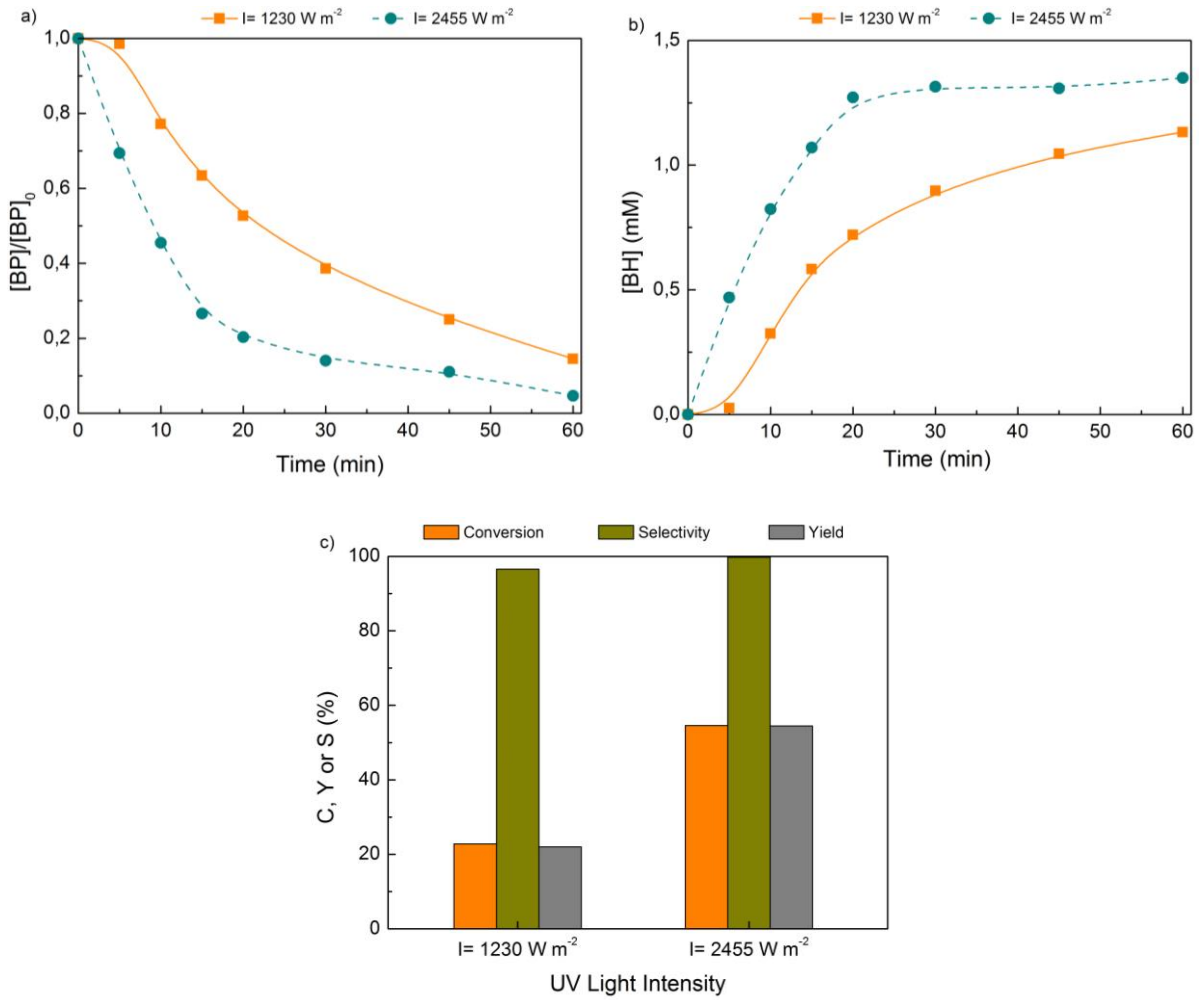


**Figure 17 -** Effect of UV light irradiance on the photocatalytic reduction of BP; $[BP]_0$=1.5 mM; [KOH]=5 mM; $TiO_2$ P25 load = 0.1 g $L^{-1}$; solvent: isopropanol: a) Normalized BP concentration profiles during the photocatalytic reduction of BP; b) BH concentration profiles during the photocatalytic reactions; c) BP conversion, yield and selectivity toward BH formation at 10 min of reaction.

**Table 7 –** Effect of irradiance (I) in the initial rate of BP reduction ($r_{i,BP}$) and BH formation ($r_{i,BH}$), using [KOH] = 5 mM and a $TiO_2$ P25 load of 0.1 g $L^{-1}$.

| **Irradiance (W $m^{-2}$)** | $r_{i,BP}$ **x $10^2$ (mM $min^{-1}$)** | $r_{i,BH}$ **x $10^2$ (mM $min^{-1}$)** |
|---|---|---|
| 1230 | 0.4 | 0.4 |
| 2455 | 6.6 | 6.3 |

### 4.2.6 Effect of the Solvent

Different solvents were also studied, under photochemical and photocatalytic conditions, to determine its efficiency toward the production of BH (Figures 18 and Figure 19, accordingly).

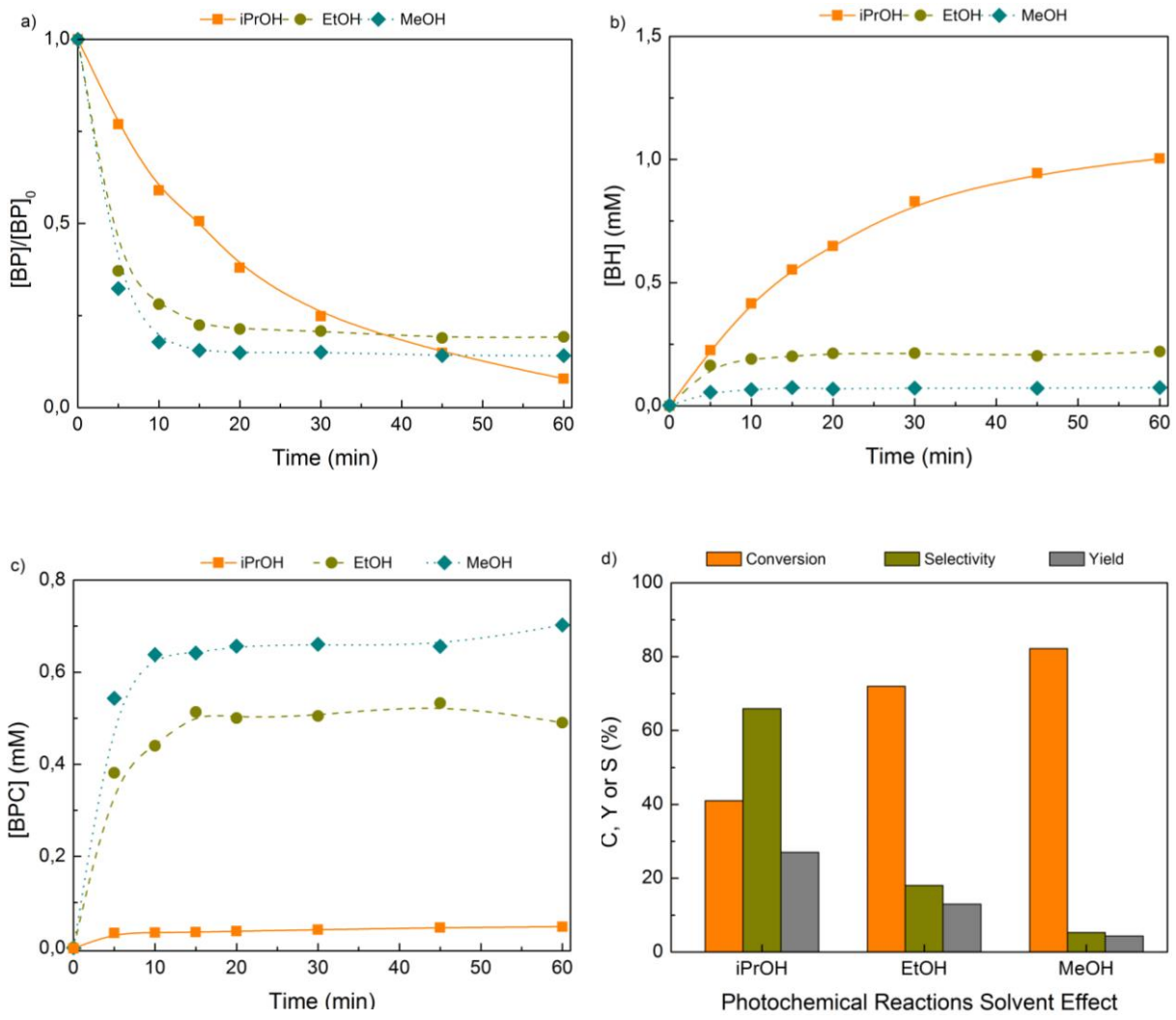


**Figure 18 -** Effect of type of solvent in the photochemical reduction of BP; $[BP]_0$=1.5 mM; [KOH]=5 mM: a) Normalized BP concentration profiles during the photochemical reduction of BP using methanol, ethanol and isopropanol; b) BH concentration profiles during the photochemical reactions; c) BPC concentration profile during the photochemical reactions; d) BP conversion, yield and selectivity toward BH formation at 10 min of reaction.

From Figures 18 a and c, it can be observed that the initial conversion of BP and formation of BPC decreases with the size of the alcoholic chain, correspondingly. Moreover, according to Figure 18 b production of BH increases following the order MeOH<EtOH<iPrOH. Although BP is slower for the reactions using iPrOH, selectivity and yield are higher. For instance, at 10 min or reaction, selectivity and

yield are close to 5% using MeOH and under 20% for EtOH, while iPrOH promoted a BH yield of 27% and a selectivity of 66% for these conditions.

Table 8 shows the initial reaction rates for these photochemical reactions, while Table 9 does so for the photocatalytic ones.

**Table 8 –** Effect of the type of solvent in the initial reaction rates of photochemical BP reduction ($r_{i,BP}$) and BH formation ($r_{i,BH}$) using [KOH] = 5 mM.

| Solvent | $r_{i,BP}$ x $10^2$ (mM $min^{-1}$) | $r_{i,BH}$ x $10^2$ (mM $min^{-1}$) |
|---|---|---|
| MeOH | 20.1 | 1.1 |
| EtOH | 18.4 | 3.3 |
| iPrOH | 6.8 | 4.2 |

From Table 8, it is thus concluded that with increasing number of methyl groups in the alcohol, there is a reduction in rate for BP degradation and a rise in BH formation. The results are in line with the availability of hydrogen in the structure of the used alcohols, since two moles of hydrogen atoms are needed for producing 1 mol of BH.

It is then demonstrated that KOH efficiently extracts hydrogen for iPrOH only, while the other solvents continuously produce the one-photon products, such as BPC. This is due to the hydrogen donating ability toward the two-photon product, which is BH, increasing with the nucleophicity of the alcohol in relation to electrophilic radicals [11].

Photocatalytic reactions were also performed, under similar conditions. From Figure 19 a, it can be observed that during the first few minutes, BP is faster converted in the presence of EtOH, followed by MeOH and finally iPrOH. Once again, iPrOH slowly converts the substrate, so that it has the lowest concentration of all in the last few samples, implying that the reaction happens at a slower rate, but more selectively toward the desired product, as shown in Figure 19 b. Also addressing Figure 19 c, EtOH seems to promote BP conversion into BPC, with small amounts of BH being formed in the process, while MeOH also produces a lesser quantity of product but the highest amount of undesired product after 15 minutes, overcoming EtOH.

Differently from the photochemical reactions evaluating solvent effect, at 10 min of irradiation, conversion is higher using EtOH (C=86%), while selectivity and yield are parallel to the photochemical reactions, being around 5% for MeOH and fewer than 20% for EtOH, while iPrOH has yield of 50% and a whopping selectivity of 97% for these conditions (Figure 19 d).

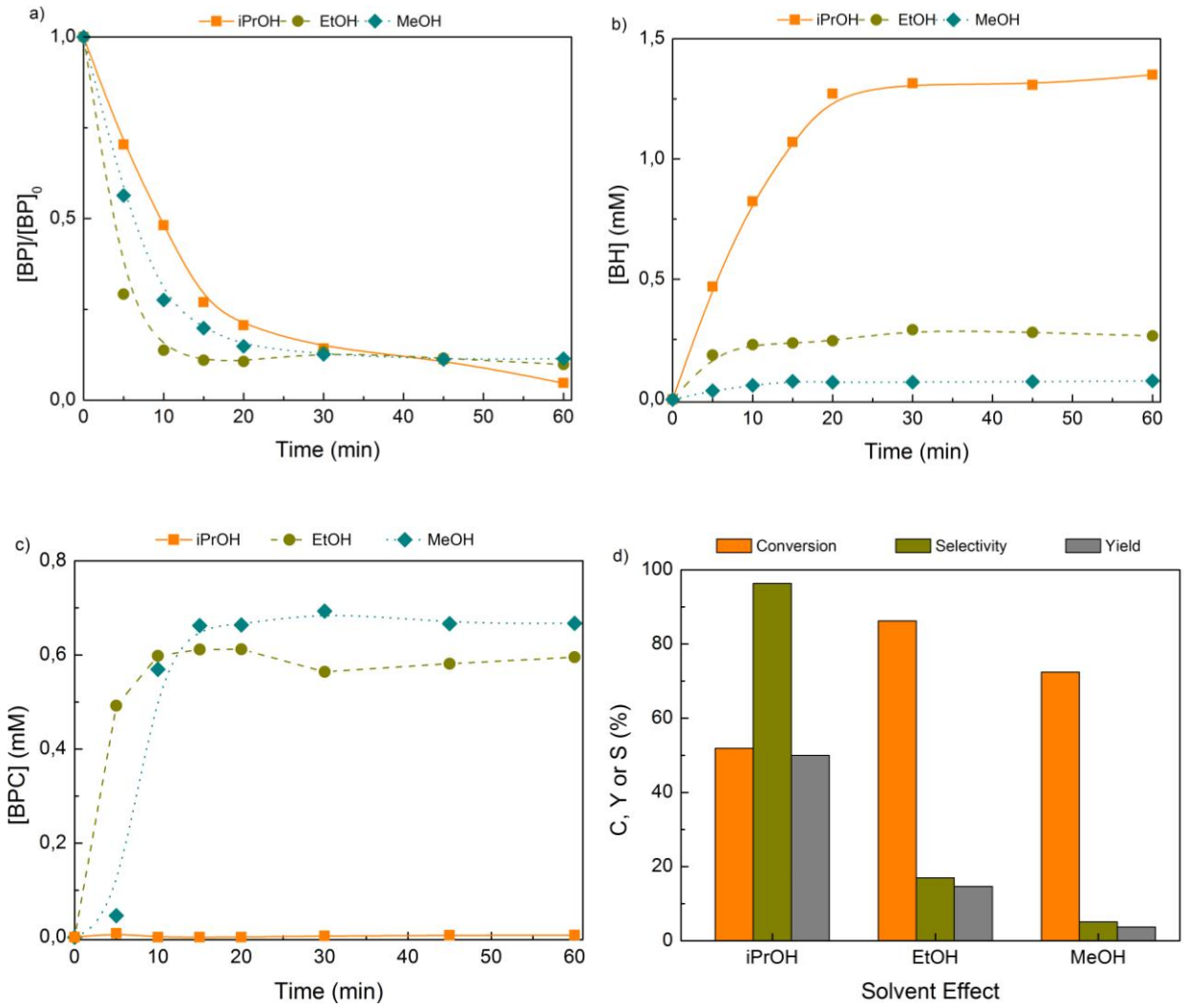


**Figure 19 -** Effect of type of solvent in the photocatalytic reduction of BP; $[BP]_0$=1.5 mM; [KOH]=5 mM; $TiO_2$ P25 load = 0.1 g $L^{-1}$: a) Normalized BP concentration profiles during the photocatalytic reduction of BP using methanol, ethanol and isopropanol; b) BH concentration profiles during the photocatalytic reactions; c) BPC concentration profile during the photocatalytic reactions; d) BP conversion, yield and selectivity toward BH formation at 10 min of reaction.

**Table 9 -** Effect of the type of solvent in the initial reaction rates of photocatalytic BP reduction ($r_{i,BP}$) and BH formation ($r_{i,BH}$) using [KOH] = 5 mM and $TiO_2$ P25 load of 0.1 g $L^{-1}$.

| **Solvent** | $r_{i,BP}$ **x 10$^2$ (mM min$^{-1}$)** | $r_{i,BH}$ **x 10$^2$ (mM min$^{-1}$)** |
|---|---|---|
| MeOH | 13.0 | 0.7 |
| EtOH | 21.2 | 3.5 |
| iPrOH | 9.1 | 9.1 |

As previously mentioned, initial reaction rates of BP reduction are higher using EtOH as solvent, followed by MeOH and iPrOH. BH initial rate formation is as expected, with the rate increasing with chain size.

The above results suggest that EtOH interacts very differently for BP reduction, under the presence of catalyst and KOH, when compared to the photochemical reaction. Once again, the presence of $TiO_2$ along with KOH appeared to be crucial for the selective production of BH form BP. Also, for photocatalytic reduction of a aldehyde with $TiO_2$, better results with the ethanolic solution and a base would be expected, according to Pross et al. [77].

### 4.2.7 Effect of type of catalyst

Gold, platinum and palladium loaded over $TiO_2$ P25 (Au/P25, Pt/P25 and Pd/P25, respectively) were used for photocatalytic reactions over the course of this work. A new promising material with semiconductor properties - graphitic carbon nitride (g-$C_3N_4$) - will be used as well, and has been known to function also under visible light conditions, with a lower band gap for the charge separation to happen, possesses very good chemical stability and endures heat. Its exceptional conformation gives it an unique electronic structure, aiding to photoassisted reactions [108].

Experiments with these different catalysts were carried out in the presence and absence of KOH (Figures 20 and 21, respectively). The initial reaction rates obtained for these reactions are listed on Tables 10 and 11. $TiO_2$ P25 was compared with commercial $TiO_2$ anatase (SA), with the respective metal-loaded $TiO_2$ P25 materials and also g-$C_3N_4$.

For the reactions in the presence of KOH, the a catalyst load of 0.1 g $L^{-1}$ was fixed for all materials since it was found as the optimal load for $TiO_2$ P25. Comparison with the photochemical reaction using the same concentration of KOH (5mM) was also performed.

From Figure 20 a, a superior performance by the $TiO_2$ P25 catalyst can be observed in terms of BP reduction. The photochemical conversion of BP was slower than for the reaction using $TiO_2$ P25, while Au/P25 and $TiO_2$ SA show even slower rates of BP reduction.

The highest efficiency of $TiO_2$ P25 catalyst is yet again observed for BH production (Figure 20 b), but in this case of the reaction using Pd/P25, a similar amount of BH was formed, followed by Pt/P25, g-$C_3N_4$ and Au/P25. The lowest amount of BH was obtained through the photochemical reaction and using $TiO_2$ SA catalyst. 100% selectivity at 10 min of reaction was attained for P25, Pt/P25 and Pd/P25. SA and the photochemical reaction have the lowest selectivities and yields of less than 70% and 35%, accordingly. The use of Au/P25 and g-$C_3N_4$ also resulted in high selectivity of c.a. 90%, which is still considered a very good result.

The reaction rates of the photocatalytic reactions are relatively high when compared with the photochemical reaction, with an increase of over 32% for the P25, Pt/P25 and Pd/P25 in the BP conversion and 112% for the BH production (Table 10). Yet the use of $TiO_2$ SA did not produce a positive effect in the rate of both BP reduction and BH formation. The above results suggest that the type of $TiO_2$ is of high importance for the efficiency of BH production; leading to $TiO_2$ P25 having what should be the best photocatalytic performance in the presence of KOH. The highest efficiency observed for $TiO_2$ may be

related to its intrinsical physical-chemical properties such as the presence of OH groups at its surface and surface area, as well as to a synergetic effect between anatase and rutile crystals leading to a high charge separation efficiency [51].

The introduction of metal nanoparticles for the photocatalytic reactions in the presence of KOH did not produce a significant effect in the efficiency of the BH production process. Among metal-loaded materials Pt/P25 and Pd/P25 were the most efficient. This may be due to the fact that catalyst load was optimized only for this catalyst. For comparison sake, catalyst load should be optimized for each of the presented semiconductors.

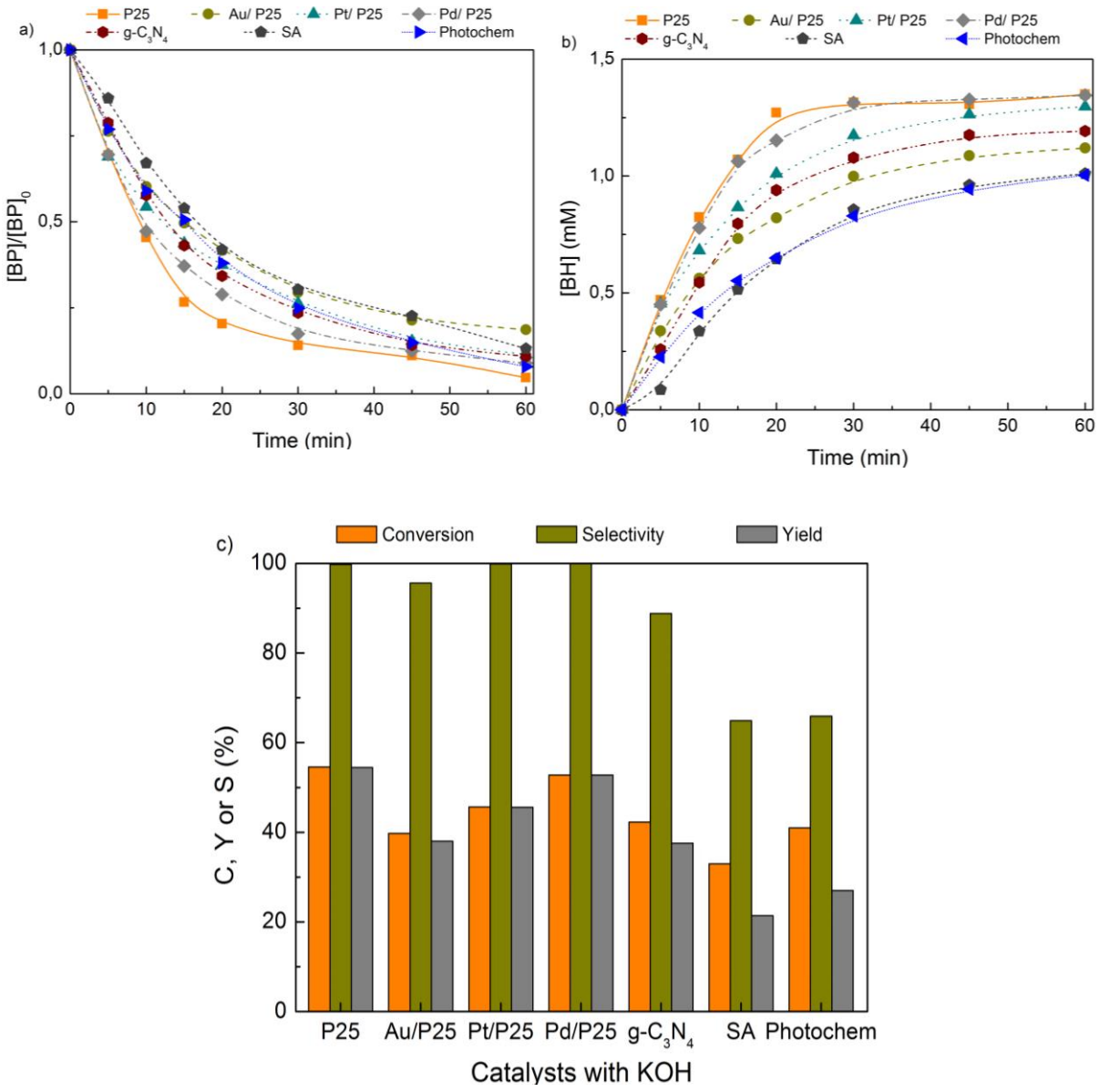


**Figure 20 -** Photocatalytic reduction of BP using different catalysts; $[BP]_0$=1.5 mM; [KOH]=5 mM; solvent: isopropanol: a) Normalized BP concentration profiles during the photocatalytic reduction of BP; b) BH concentration profiles during the photocatalytic reactions; c) BP conversion, yield and selectivity toward BH formation at 10 min of reaction.

**Table 10 -** Initial reaction rates for BP reduction ($r_{i,BP}$) and BH formation ($r_{i,BH}$) for the photocatalytic reactions using different catalysts, [KOH] = 5 mM and catalyst load of 0.1 g $L^{-1}$.

| Catalysts | $r_{i,BP}$ x $10^2$ (mM $min^{-1}$) | $r_{i,BH}$ x $10^2$ (mM $min^{-1}$) |
|---|---|---|
| P25 | 9.1 | 9.1 |
| Au/P25 | 7.0 | 6.7 |
| Pt/P25 | 9.3 | 9.1 |
| Pd/P25 | 9.0 | 8.9 |
| g-$C_3N_4$ | 6.1 | 5.1 |
| SA | 4.3 | 1.5 |
| none (photochemical) | 6.8 | 4.2 |

For the photocatalytic reactions in the absence of KOH, a catalyst load of 1 g $L^{-1}$ was used so that the effect of the introduction of KOH in the system would be more expressive. These experiments were compared with the corresponding photochemical reaction and photocatalytic reaction using a $TiO_2$ P25 load of 1 g $L^{-1}$.

In this case, a faster conversion of BP was observed when compared with the previous study in the presence of KOH (Figure 21 a). It is worth noticing that both P25 0.1 g $L^{-1}$ and Pd/P25 still hold the best results in terms of BP conversion. Remarkably, the g-$C_3N_4$ and $TiO_2$ P25 with the highest load have declined on this parameter. The photochemical reaction is one of the quickest, and converts BP even at a higher pace, when compared with the previous study.

As shown in Figure 21 b, production of BH is substantially lower than that obtained for the reactions with KOH. The highest amount of product was formed using Pd/P25 and Pt/P25, followed by P25 1 g $L^{-1}$ and then the by the photochemical reaction. g-$C_3N_4$ yielded the smallest amount of BH, but appears to have improved performance under KOH presence, when compared with other catalysts.

In the absence of KOH, BPC formation was the highest for the photochemical reaction, reaching a little over 0.75 mM at the end of the reaction, and then SA and Au/P25 with close to 0.7 mM (Figue 21 c). The amount of BPC formed in the reactions using $TiO_2$ P25 as catalyst did not differ significantly by changing the catalyst load, with close to 0.7 mM being obtained at the end of the reaction. Pd/P25 and Pt/P25 produced the lowest amounts, ranging from 0.4 to 0.6 mM.

From Figure 21 d, P25 1 g $L^{-1}$, g-$C_3N_4$ and Pt/P25 show the lower conversions, going from 60% to 70%. This is almost 15 to 20% lower than the BP conversion obtained for all the other reactions, ensuring that these catalysts have low rate of reaction on the first few moments of reaction (Table 11). $TiO_2$ P25 and the Pt/P25 catalyst have two of the highest selectivities and yields, only to be overcomed by Pd/P25, which resulted in 88% of BP conversion and 25% selectivity and 22% yield toward BH formation.

Even though the photochemical reaction holds great values in face to the photocatalytic reactions, with 86%, 12% and 11% of conversion, selectivity and yield, respectively, there is the formation of immense amounts of BPC, which constitutes a drawback.

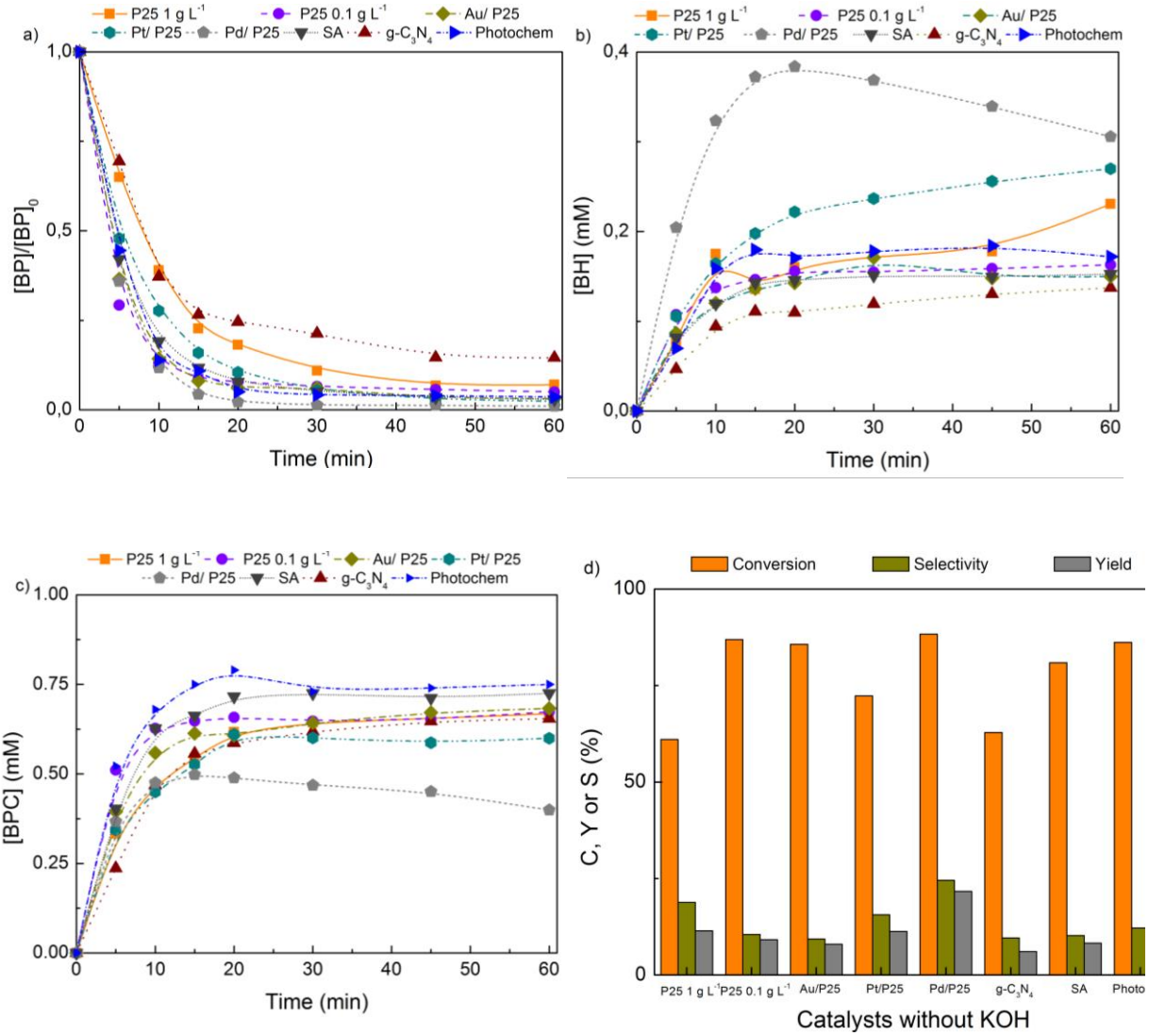


**Figure 21 -** Photocatalytic reduction of BP using different catalysts without KOH; $[BP]_0$=1.5 mM; solvent: isopropanol: a) Normalized BP concentration profiles during the photocatalytic reduction of BP; b) BH concentration profiles during the photocatalytic reactions; c) BPC concentration profile during the photocatalytic reactions; d) BP conversion, yield and selectivity toward BH formation at 10 min.

It was also found that for the reactions using metal-loaded $TiO_2$ in the absence of KOH some unidentified peaks of small relative areas were observed in the HPLC chromatograms, which may indicate the exhistence of a different in mechanism [102, 109]. It is generally accepted that upon irradiation of $TiO_2$, noble metals act as electron trapping centers and promote the electron–hole separation, being expected an enhancement in the activity for photoreduction [53].

**Table 11 -** Initial velocities for the reduction of BP ($r_{i,BP}$) and BH formation ($r_{i,BH}$) for the photocatalytic reactions in the absence of KOH and a load of 1 g $L^{-1}$, unless stated otherwise.

| Catalysts | $r_{i,BP}$ x $10^2$ (mM $min^{-1}$) | $r_{i,BH}$ x $10^2$ (mM $min^{-1}$) |
|---|---|---|
| P25 | 10.5 | 1.5 |
| P25 0.1 g $L^{-1}$ | 21.3 | 2.1 |
| Au/P25 | 18.7 | 1.7 |
| Pt/P25 | 15.2 | 2.1 |
| Pd/P25 | 19.1 | 4.1 |
| g-$C_3N_4$ | 9.1 | 0.8 |
| SA | 16.7 | 1.6 |
| none (Photochemical) | 16.8 | 1.4 |

The reaction rate of BH formation is substancially lower than those obtained for the reactions in the presence of KOH, while BPC is formed in mensurable amounts. These results suggest that both photochemical and photocatalytc routes can play a role and that the presence of a hydrogen abstraction agent is crucial for the selective production of BH from BP. Additionaly, for BH formation under the absence of KOH, the reaction using Pd/P25 shows the best result, which could be attributed to the improved UV absorbance, although these should not be active for higher wavelengths. Pd nanoparticles are capable of adsorbing hydrogen at its surface and are normally used in photocatalytic reduction reactions [110], which may be another of the reason for the good performance of Pd/P25. g-$C_3N_4$, although not the most effective under UV light conditions, may be a promising option for visible light reactions. However, further studies should be performed. $TiO_2$ SA, which is mainly constituted by anatase, show less efficiency than P25 from Evonik® Degussa, proving that differences in crystalline strucutres have shown to be the determining factor for both this chain of reactions and the former series with KOH [51].

The surface area of the photocatalysts (Table 2) are in accordance with the obtained results, since P25 is a much better catalyst than SA and g-$C_3N_4$, while these two latter ones seem to have similar $S_{BET}$, and therefore less active sites for adsorption and reaction to take place.

Once again, since different catalysts were used, the catalyst load should be optimized in order to have the optimized performance for each of the materials.

### 4.2.8 Photochemical and photocatalytic conversion of BP into BH under simulated solar light irradiation

Reactions for simulating outdoor conditions using a Xe lamp were performed, in order to evaluate if the reactions are propense to happen using Sun as irradiation source. Figure 22 shows the results of those experiments. Simulated solar light was addressed as SSL at this point.

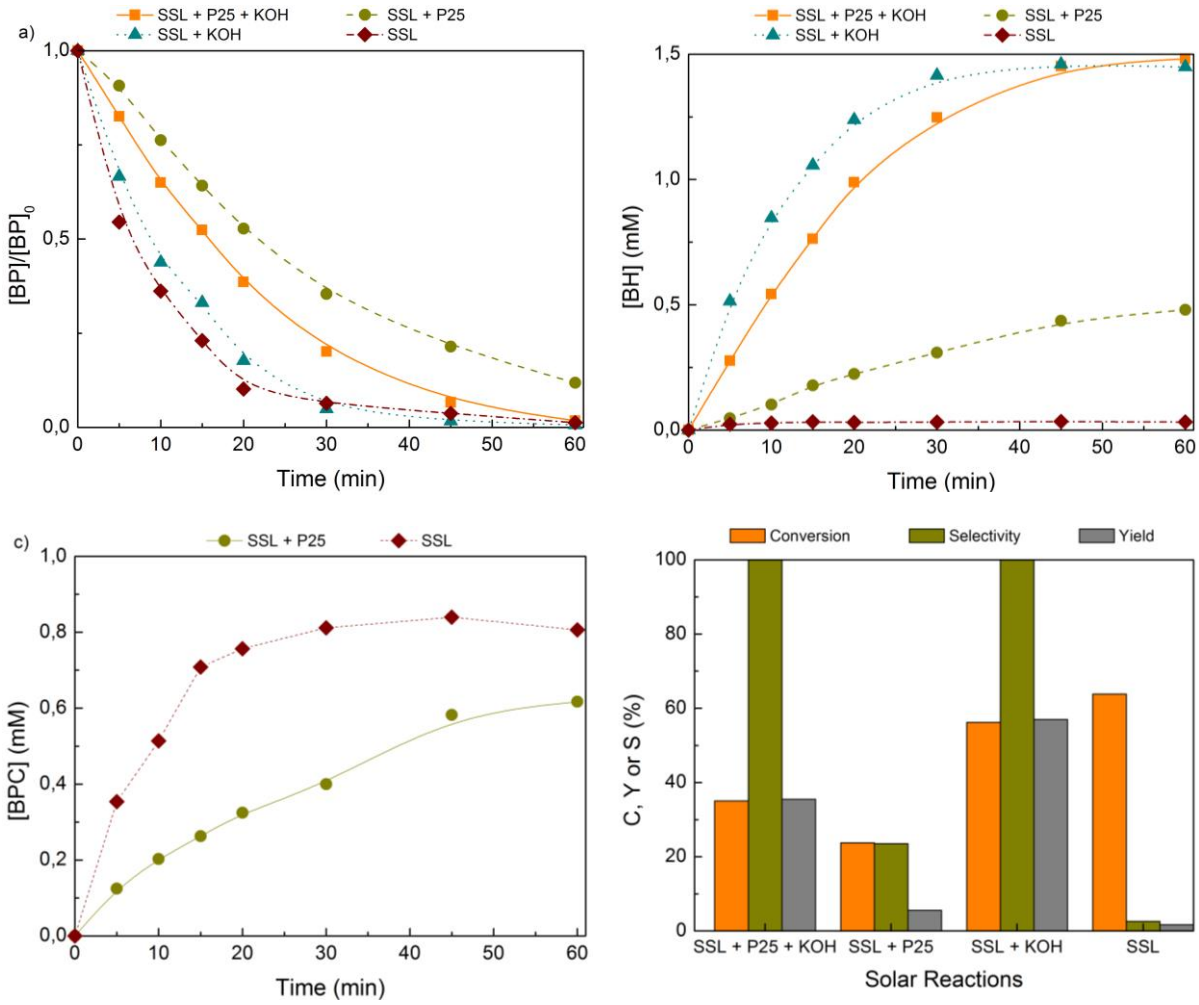


**Figure 22 -** Photocatalytic and photocatalytic reduction of BP under simulated solar light irradiation; $[BP]_0$=1.5 mM; [KOH]=5 mM; solvent: isopropanol: a) Normalized BP concentration profiles during the reduction of BP; b) BH concentration profiles during the photoinitiated reactions; c) BPC concentration profile during the photoinitiated reactions; d) BP conversion, yield and selectivity toward BH formation at 10 min of reaction.

From Figure 22 a it can be observed that, excluding the case of the photocatalytic reaction without KOH, the reaction is complete in less than 60 minutes. The fastest BP reduction was attained for the photochemical reaction, followed by the photochemical reaction in the presence of KOH, the photocatalytic reaction using KOH and finally, the photocatalytic reaction in the absence of KOH. Considering BH production (Figure 22 b), the reactions with KOH were complete, i.e. all BP was converted into BH, and for those without KOH, lower amounts of BH were produced. Figure 22 c shows

the BPC concentration profile during the reactions, with no BPC being formed in the presence of KOH. Finally, Figure 22 d shows that selectivity at 10 min of reaction was absolute for the reactions using KOH, reaching 23% for the photocatalytic and 2% for the photochemical reactions in the absence of KOH. Conversion shows the same tendency as that was observed in Figure 22 a. Yield is highest for the reaction solely with KOH, followed by the photocatalytic with KOH, the photocatalytic without KOH and the simply photochemical reaction.

The initial reaction rates for BP conversion and BH formation are listed in Table 12.

**Table 12 -** Initial reaction rates for BP reduction ($r_{i,BP}$) and BH formation ($r_{i,BH}$) for the reactions under simulated solar light (SSL) irradiation using [KOH] = 5 mM and a $TiO_2$ P25 load of 1 g $L^{-1}$.

| Reaction conditions | $r_{i,BP}$ x $10^2$ (mM $min^{-1}$) | $r_{i,BH}$ x $10^2$ (mM $min^{-1}$) |
|---|---|---|
| SSL + P25 + KOH | 5.1 | 5.1 |
| SSL + P25 | 2.8 | 0.6 |
| SSL + KOH | 10.0 | 10.0 |
| SSL | 13.5 | 0.4 |

It may be concluded that the reaction may be performed efficiently under solar outdoor conditions. Besides, KOH allows for the selective transformation of substrate into BH, while the catalyst seems to delay the formation of this product. Without KOH, initial reaction rate is quite slow, very close to the one for the photochemical reaction without KOH.

# 5 Conclusion

A method of producing benzhydrol (BH) through the photochemical and photocatalytic reduction of benzophenone (BP) using UV-LEDs which exhibit high efficiency to power ratio, low cost, with easily producible catalysts with low to no toxicity and in a short amount of reaction time. A range of parameters such as the presence and type of catalyst, catalyst load, BP initial concentration, irradiance and presence of the potassium hydroxide (KOH) affected the desired product formation.

An optimal catalyst load for titanium dioxide ($TiO_2$) P25 from Evonik® Degussa was found to be 0.1 g $L^{-1}$.

A minimal amount of KOH, was utilized to facilitate hydrogen abstraction from the isopropanol - which was used as solvent and hole scavenger - ensuring that selectivity toward BH is high and there is not an excess of hydroxide anions. A KOH concentration of 5 mM provide the best compromise between yield and selectivity (Y=55%; S=100% at 10 minutes of reaction), but further study into the optimization of this parameter should be made from the green chemistry point of view, since further lowering of the amount of KOH would be environmentally beneficial and would only have a minor effect on the reaction rate and results. BPC was found as by-product only in the reactions using less than 1 mM KOH.

Controlling the initial concentration of BP substrate, a competition between the photochemical reaction was found, favored at high concentrations of BP and the photocatalytic reaction, which is higher at low concentrations.

UV light intensity was addressed for this photocatalytic reaction, showing that the formation of the two-photon product (BH) is proportional to the irradiance of the UV-LEDs in the range studied in this work. Reaction rate, conversion and yield also varied similarly to the intensity of the irradiation source.

For both the photochemical and photocatalytic reactions, different solvents (alcohols) were used, namely methanol, ethanol and isopropanol. Initial conversion of BP and formation of undesired products diminishes with increasing degree of number of methyl groups of the alcohol, while BH production increases. This behavior was attributed to the nucleophilical properties of the alcohols, which serve as hydrogen donors. iPrOH provided the best results in terms of yield and selectivity toward the production of BH.

Different catalysts, with dispar sorts of $TiO_2$ crystaline structures, noble metal (Au, Pt and Pd) loaded $TiO_2$ and graphitic carbon nitride (g-$C_3N_4$) were also tested for the production of BH in the presence and in the absence of KOH. The best results for the evaluated catalysts, were obtained for the Pd-loaded $TiO_2$ P25 from Evonik® Degussa, with 25% selectivity and 22% yield in the absence of KOH, and for 0.1 g $L^{-1}$ $TiO_2$ P25 from Evonik® Degussa, with 54% conversion and yield and 100% in selectivity in the presence of KOH (at 10 min of irradiation). It is a more efficient way of producing BH than the photochemical reaction, which only has a similar BP conversion but a difference in over 10% in selectivity and yield in the absence of KOH, and 25% in the presence of this compound. About 35 to 75% more BH is formed throughout the photocatalytic process for the reaction with and without KOH, respectively.

Reactions with simulated solar light were also performed, to see whether the reaction is feasible under sunlight. It was found that it is very effective under these conditions, especially for the case of the

photochemical reaction with KOH, where a 57% yield with 100% selectivity were achieved after 10 minutes of reaction.

From the work performed, it may be concluded that under certain conditions, the photocatalytic reaction is more efficient than the photochemical. Yet, the presence of KOH is the determining factor for the selective sole production of BH either for the photochemical or the photocatalytic reaction, by ensuring hydrogen abstraction from the hole scavenger.

Overall, the photocatalytic reaction using $TiO_2$ P25 as catalyst under UV-LED irradiation, in the presence of KOH and using iPrOH as solvent/hole scavenger yielded the best results by efficiently producing the intended compound. Under simulated solar light, the optimal results were obtained for the photochemical reaction with a 5 mM concentration of KOH.

## 5.1 Limitations and Future Work

Further studies aiming at the complete absence of the potassium hydroxide salt should be performed.

Modifications of the catalyst should be attempted in order to take additional advantage of the solar spectrum, aiming to perform not only under UV light conditions, but also under visible light conditions. Following that, the process could be effectively implemented in an industrial context.

Also, it would be worthwhile to investigate the possibility of formation of secondary products besides benzopinacol (for instance by UPLC-MS), with further quantification for an efficient separation and mechanistic study.

On the topic of solvents, more hole scavengers could be tested in the absence of KOH, namely amines such as trimethylamine, to evaluate its performance as a sole hole scavenger.

Recycling the solvent and reutilizing the catalyst are two additional suggestions. Employment of catalyst on a fixed bed would be an efficient way of avoiding catalyst separation and making it possible to operate under continuous reaction conditions.

Reactions under solar simulated conditions should be performed using other catalysts, namely palladium and platinum based catalysts, since these had very promising results under UV conditions and exhibit surface plasmon resonance (SPR) effect, which may have a positive effect for reactions under visible light irradiation. Some other favorable catalysts worth testing, especially under simulated solar light, would be the already addressed cadmium sulfide (CdS) [45-47] and CdS impregnated on a graphitic carbon nitride ($CdS/g\text{-}C_3N_4$) composite [111, 112], due to their capacity of being excited by the visible part of the solar spectrum. Coupling carbon materials with $TiO_2$ would be another interesting feature to add to existing catalysts, by increasing the surface area and enhance the electronic properties of the semiconductor [113]. Sonification techniques and different proportions of $TiO_2$ crystal and its effect on the photocatalytic reaction are another matter worth studying.

Lastly, further studies into the mechanism and kinetic of the photocatalytic processes should also be performed.

# References


1. Hoffert, M.I., *Farewell to Fossil Fuels?* Science, 2010. **329**(5997): p. 1292-1294.
2. Mackey, B. and D. Lindenmayer, *Fossil fuels' future.* Science, 2014. **345**(6198): p. 739-740.
3. Townsend, M., *energy rush.* Geographical (Campion Interactive Publishing), 2002. **74**(5): p. 38.
4. Kalyanasundaram, K. and M. Graetzel, *Artificial photosynthesis: biomimetic approaches to solar energy conversion and storage.* Current Opinion in Biotechnology, 2010. **21**(3): p. 298-310.
5. Ibhadon, A. and P. Fitzpatrick, *Heterogeneous Photocatalysis: Recent Advances and Applications.* Catalysts, 2013. **3**(1): p. 189.
6. Protti, S. and M. Fagnoni, *The sunny side of chemistry: green synthesis by solar light.* Photochemical & Photobiological Sciences, 2009. **8**(11): p. 1499-1516.
7. Spasiano, D., R. Marotta, S. Malato, P. Fernandez-Ibañez, and I. Di Somma, *Solar photocatalysis: Materials, reactors, some commercial, and pre-industrialized applications. A comprehensive approach.* Applied Catalysis B: Environmental, 2015. **170–171**: p. 90-123.
8. Hunt, V., N. Manson, and P. Morgan, *A wake-up call for Big Pharma*, in *Mckinsey & Company*. 2011.
9. Choursina, K. and S. Kravchenko, *China's Drug-Price Cuts Are Hitting Big Pharma Where It Hurts*, in *Bloomberg*. 2016.
10. Anastas, P. and N. Eghbali, *Green Chemistry: Principles and Practice.* Chemical Society Reviews, 2010. **39**(1): p. 301-312.
11. Adam, W. and B. Walther, *Multiple-photon chemistry in the benzophenone photoreduction during laser-jet photolysis: Effect of alcohol solvent on cross-coupling versus hydrogen abstraction of the electronically excited hydroxydiphenylmethyl radical.* Tetrahedron, 1996. **52**(31): p. 10399-10404.
12. Bäckstrom, H. and K. Sandros, *Transfer of triplet-state energy in fluid solutions. I. Sensitized phosphorescence and its application to the determination of triplet-state lifetimes.* Acta Chemica Scandinavica, 1960. **14**: p. 48-62.
13. Demeter, A. and T. Bérces, *Study of the long-lived intermediate formed in the photoreduction of benzophenone by isopropyl alcohol.* Journal of Photochemistry and Photobiology A: Chemistry, 1989. **46**(1): p. 27-40.
14. Demeter, A., K. Horváth, K. Böőr, L. Molnár, T. Soós, and G. Lendvay, *Substituent Effect on the Photoreduction Kinetics of Benzophenone.* The Journal of Physical Chemistry A, 2013. **117**(40): p. 10196-10210.
15. Demeter, A., B. László, and T. Bérces, *Kinetics of Ketyl Radical Reactions Occurring in the Photoreduction of Benzophenone by Isopropyl Alcohol.* Berichte der Bunsengesellschaft für physikalische Chemie, 1988. **92**(12): p. 1478-1485.
16. Den Hollander, J.A., A.J. Hartel, and P.H. Schippers, *CIDNP study of the photoreduction of benzophenone with secondary alcohols.* Tetrahedron, 1977. **33**(2): p. 211-215.
17. Moore, W.M., G.S. Hammond, and R.P. Foss, *Mechanisms of Photoreactions in Solutions. I. Reduction of Benzophenone by Benzhydrol.* Journal of the American Chemical Society, 1961. **83**(13): p. 2789-2794.

18. Moore, W.M. and M.D. Ketchum, *The Limiting Quantum Yield for the Photoreduction of Benzophenone with Isopropyl Alcohol.* The Journal of Physical Chemistry, 1964. **68**(1): p. 214-217.
19. Naguib, Y.M.A., S.G. Cohen, and C. Steel, *Reduction of crystal violet by diphenylketyl radicals.* Journal of the American Chemical Society, 1986. **108**(1): p. 128-133.
20. Pitts, J.N., R.L. Letsinger, R.P. Taylor, J.M. Patterson, G. Recktenwald, and R.B. Martin, *Photochemical Reactions of Benzophenone in Alcohols1.* Journal of the American Chemical Society, 1959. **81**(5): p. 1068-1077.
21. Viltres Costa, C., M.A. Grela, and M.S. Churio, *On the yield of intermediates formed in the photoreduction of benzophenone.* Journal of Photochemistry and Photobiology A: Chemistry, 1996. **99**(1): p. 51-56.
22. Ravelli, D., D. Dondi, M. Fagnoni, and A. Albini, *Photocatalysis. A multi-faceted concept for green chemistry.* Chemical Society Reviews, 2009. **38**(7): p. 1999-2011.
23. Albiter Escobar, E., M.Á. Valenzuela Zapata, S. Alfaro Hernández, S.O. Flores Valle, O. Ríos Berny, V.J. González Ángeles, and I. Córdova Reyes, *Photocatalytic Reduction of Benzophenone on $TiO_2$: Effect of Preparation Method and Reaction Conditions.* Journal of the Mexican Chemical Society, 2010. **54**: p. 133-138.
24. Armaroli, N. and V. Balzani, *The Future of Energy Supply: Challenges and Opportunities.* Angewandte Chemie International Edition, 2007. **46**(1-2): p. 52-66.
25. Zou, Z., J. Ye, K. Sayama, and H. Arakawa, *Direct splitting of water under visible light irradiation with an oxide semiconductor photocatalyst.* Nature, 2001. **414**(6864): p. 625-627.
26. Yu, J., P. Zhang, H. Yu, and C. Trapalis, *Environmental Photocatalysis.* International Journal of Photoenergy, 2012. **2012**: p. 4.
27. Noël, T., *Chemical photocatalysis*, in *Green Processing and Synthesis*. 2013. p. 531.
28. Ravelli, D., M. Fagnoni, and A. Albini, *Photoorganocatalysis. What for?* Chemical Society Reviews, 2013. **42**(1): p. 97-113.
29. Ravi, S.K. and S.C. Tan, *Progress and perspectives in exploiting photosynthetic biomolecules for solar energy harnessing.* Energy & Environmental Science, 2015. **8**(9): p. 2551-2573.
30. *Electricity net generation: electric power sector, 1949-2012*. Energy Information Administration 2016; Available from: http://www.eia.gov/.
31. *Industrial Consumption Energy Consumption Estimates, 1949-2012*. Energy Information Administration 2016; Available from: http://www.eia.gov/.
32. Lang, X., X. Chen, and J. Zhao, *Heterogeneous visible light photocatalysis for selective organic transformations.* Chemical Society Reviews, 2014. **43**(1): p. 473-486.
33. Fujishima, A., K. Nakata, T. Ochiai, A. Manivannan, and D.A. Tryk, *Recent Aspects of Photocatalytic Technologies for Solar Fuels, Self-Cleaning, and Environmental Cleanup.* Electrochemical Society Interface, 2013: p. 51.
34. Braslavsky, S.E., *Glossary of terms used in photochemistry 3rd edition (IUPAC Recommendations 2006).* Pure and Applied Chemistry, 2007. **79**(3).
35. Fox, M.A. and M.T. Dulay, *Heterogeneous photocatalysis.* Chemical Reviews, 1993. **93**(1): p. 341-357.

36. Fujishima, A. and K. Honda, *Electrochemical Photolysis of Water at a Semiconductor Electrode.* Nature, 1972. **238**(5358): p. 37-38.
37. Silva, C.G., R. Juárez, T. Marino, R. Molinari, and H. García, *Influence of Excitation Wavelength (UV or Visible Light) on the Photocatalytic Activity of Titania Containing Gold Nanoparticles for the Generation of Hydrogen or Oxygen from Water.* Journal of the American Chemical Society, 2011. **133**(3): p. 595-602.
38. Kohtani, S. and H. Miyabe, *Titanium Dioxide-Induced Photocatalytic Reduction for Organic Synthesis.* Chemical Physics Research Journal, 2014. **7**(1).
39. Silva, C.G. and J.L. Faria, *Effect of key operational parameters on the photocatalytic oxidation of phenol by nanocrystalline sol–gel $TiO_2$ under UV irradiation.* Journal of Molecular Catalysis A: Chemical, 2009. **305**(1–2): p. 147-154.
40. Vijaikumar, S., N. Somasundaram, and C. Srinivasan, *Photoinduced oxidation of benzhydrol and reduction of benzil on titanium dioxide.* Applied Catalysis A: General, 2002. **223**(1–2): p. 129-135.
41. Gaya, U.I. and A.H. Abdullah, *Heterogeneous photocatalytic degradation of organic contaminants over titanium dioxide: A review of fundamentals, progress and problems.* Journal of Photochemistry and Photobiology C: Photochemistry Reviews, 2008. **9**(1): p. 1-12.
42. Nakata, K. and A. Fujishima, *$TiO_2$ photocatalysis: Design and applications.* Journal of Photochemistry and Photobiology C-Photochemistry Reviews, 2012. **13**(3): p. 169-189.
43. Roper, D.K., W. Ahn, and M. Hoepfner, *Microscale Heat Transfer Transduced by Surface Plasmon Resonant Gold Nanoparticles.* The Journal of Physical Chemistry C, 2007. **111**(9): p. 3636-3641.
44. Hasegawa, M.C., J.F.d.S. Daniel, K. Takashima, G.A. Batista, and S.M.C.P. da Silva, *COD removal and toxicity decrease from tannery wastewater by zinc oxide-assisted photocatalysis: a case study.* Environmental Technology, 2014. **35**(13): p. 1589-1595.
45. Shiragami, T., H. Ankyu, S. Fukami, C. Pac, S. Yanaglda, H. Mori, and H. Fujita, *Semiconductor photocatalysis: visible light induced photoreduction of aromatic ketones and electron-deficient alkenes catalysed by quantised cadmium sulfide.* Journal of the Chemical Society, Faraday Transactions, 1992. **88**(7): p. 1055-1061.
46. Shiragami, T., C. Pac, and S. Yanagida, *Nonmetallised CdS-catalysed photoreduction of aromatic ketones to alcohols and/or pinacols.* Journal of the Chemical Society, Chemical Communications, 1989(13): p. 831-832.
47. Shiragami, T., C. Pac, and S. Yanagida, *Visible-light-induced two-electron-transfer photoreductions on cadmium sulfide: effects of morphology.* The Journal of Physical Chemistry, 1990. **94**(2): p. 504-506.
48. Kamat, P.V., *$TiO_2$ Nanostructures: Recent Physical Chemistry Advances.* The Journal of Physical Chemistry C, 2012. **116**(22): p. 11849-11851.
49. Lazar, M., S. Varghese, and S. Nair, *Photocatalytic Water Treatment by Titanium Dioxide: Recent Updates.* Catalysts, 2012. **2**(4): p. 572.
50. Kohtani, S., E. Yoshioka, and H. Miyabe, *Hydrogenation*, ed. I. Karamé. 2012.

51. Ohno, T., K. Sarukawa, K. Tokieda, and M. Matsumura, *Morphology of a $TiO_2$ Photocatalyst (Degussa, P-25) Consisting of Anatase and Rutile Crystalline Phases.* Journal of Catalysis, 2001. **203**(1): p. 82-86.
52. *Crystal Structure Gallery*. [cited 2016 July 21]; Available from: http://www.chemtube3d.com.
53. Chen, T., Z. Feng, G. Wu, J. Shi, G. Ma, P. Ying, and C. Li, *Mechanistic Studies of Photocatalytic Reaction of Methanol for Hydrogen Production on Pt/$TiO_2$ by in situ Fourier Transform IR and Time-Resolved IR Spectroscopy.* The Journal of Physical Chemistry C, 2007. **111**(22): p. 8005-8014.
54. Molinari, R., C. Lavorato, and P. Argurio, *Photocatalytic reduction of acetophenone in membrane reactors under UV and visible light using $TiO_2$ and Pd/$TiO_2$ catalysts.* Chemical Engineering Journal, 2015. **274**: p. 307-316.
55. Su, F.-Z., L. He, J. Ni, Y. Cao, H.-Y. He, and K.-N. Fan, *Efficient and chemoselective reduction of carbonyl compounds with supported gold catalysts under transfer hydrogenation conditions.* Chemical Communications, 2008(30): p. 3531-3533.
56. Zhu, H., X. Ke, X. Yang, S. Sarina, and H. Liu, *Reduction of Nitroaromatic Compounds on Supported Gold Nanoparticles by Visible and Ultraviolet Light.* Angewandte Chemie International Edition, 2010. **49**(50): p. 9657-9661.
57. Yang, J., D. Wang, H. Han, and C. Li, *Roles of Co-catalysts in Photocatalysis and Photoelectrocatalysis.* Accounts of Chemical Research, 2013. **46**(8): p. 1900-1909.
58. Martin, D.J., *Investigation into High Efficiency Visible Light Photocatalysts for Water Reduction and Oxidation*. 2015: Springer International Publishing.
59. Chien, S.-H., M.-C. Kuo, C.-H. Lu, and K.-N. Lu, *Spectroscopic studies of NO reduction on Pt/$TiO_2$ catalysts.* Catalysis Today, 2004. **97**(2–3): p. 121-127.
60. Sin, J.-C., S.-M. Lam, K.-T. Lee, and A.R. Mohamed, *Photocatalytic performance of novel samarium-doped spherical-like ZnO hierarchical nanostructures under visible light irradiation for 2,4-dichlorophenol degradation.* Journal of Colloid and Interface Science, 2013. **401**: p. 40-49.
61. Yakabe, S., M. Hirano, J. H. Clark, and T. Morimoto, *Simple Reduction of Various Ketones with Sodium Tetrahydroborate and Alumina in Hexane.* Journal of Chemical Research, Synopses, 1998(6): p. 322-323.
62. Bawane, S.P. and S.B. Sawant, *Kinetics of Liquid-Phase Catalytic Hydrogenation of Benzophenone to Benzhydrol.* Organic Process Research & Development, 2003. **7**(5): p. 769-773.
63. Carroll, G.T., N.J. Turro, and J.T. Koberstein, *Patterning dewetting in thin polymer films by spatially directed photocrosslinking.* Journal of Colloid and Interface Science, 2010. **351**(2): p. 556-560.
64. Knowland, J., E.A. McKenzie, P.J. McHugh, and N.A. Cridland, *Sunlight-induced mutagenicity of a common sunscreen ingredient.* Federation of European Biochemical Studies Letters, 1993. **324**(3): p. 309-313.
65. IARC, *Benzophenone*. 2010, International Agency for Research on Cancer: IARC Monographs 101.

66. Brooks, A.C., P.N. Gaskell, and L.L. Maltby, *Importance of Prey and Predator Feeding Behaviors for Trophic Transfer and Secondary Poisoning.* Environmental Science & Technology, 2009. **43**(20): p. 7916-7923.
67. Kim, S. and K. Choi, *Occurrences, toxicities, and ecological risks of benzophenone-3, a common component of organic sunscreen products: A mini-review.* Environment International, 2014. **70**: p. 143-157.
68. Kerdivel, G., R. Le Guevel, D. Habauzit, F. Brion, S. Ait-Aissa, and F. Pakdel, *Estrogenic Potency of Benzophenone UV Filters in Breast Cancer Cells: Proliferative and Transcriptional Activity Substantiated by Docking Analysis.* PLoS ONE, 2013. **8**(4): p. e60567.
69. Liaw, D.-J., B.-Y. Liaw, B. Sillion, R. Mercier, R. Thiria, and H. Sekiguchi, *Synthesis and characterization of novel benzhydrol-containing poly(amide-imide)s.* Polymer International, 1999. **48**(6): p. 473-478.
70. Hashemi-Moghaddam, H. and M.R. Alaeian, *Synthesis of Molecularly Imprinted Polymer for Removal of Effective Impurity (Benzhydrol) from Diphenhydramine Hydrochloride Drug.* Journal of the Chinese Chemical Society, 2014. **61**(6): p. 643-648.
71. Ciamician, G. and P. Silber, *Chemische Lichtwirkungen.* Berichte der deutschen chemischen Gesellschaft, 1901. **34**(2): p. 1530-1543.
72. Cohen, S.G., A.W. Rose, P.G. Stone, and A. Ehret, *Competitive processes in retardation by mercaptans of photoreduction by alcohols.* Journal of the American Chemical Society, 1979. **101**(7): p. 1827-1832.
73. Valenzuela, M.A., E. Albiter, O. Ríos-Bernÿ, I. Córdova, and S.O. Flores, *Photocatalytic Reduction of Organic Compounds.* Journal of Advanced Oxidation Technologies, 2010. **13**(3): p. 321-340.
74. Murray, T.J. and D.L. Vines, *Low temperature cure using benzopinacol polymerization initiator*. 2014, Google Patents.
75. Mel'nik, V.I., K.I. Nelipovich, A.N. Faidysh, and L.B. Yankovskaya, *Fluorescence of the benzopinacol-benzophenone system and the influence of UV irradiation on it.* Journal of Applied Spectroscopy, 1980. **33**(4): p. 1075-1080.
76. Cuendet, P. and M. Graetzel, *Direct photoconversion of pyruvate to lactate in aqueous titanium dioxide dispersions.* The Journal of Physical Chemistry, 1987. **91**(3): p. 654-657.
77. Joyce-Pruden, C., J.K. Pross, and Y. Li, *Photoinduced reduction of aldehydes on titanium dioxide.* The Journal of Organic Chemistry, 1992. **57**(19): p. 5087-5091.
78. Anpo, M. and P.V. Kamat, *Environmentally benign photocatalysts: applications of titanium oxide-based materials*. 2010: Springer Science & Business Media.
79. Kalinowski, M.K., Z.R. Grabowski, and B. Pakula, *Reactivity of ketyl free radicals. Part 1.-Acid dissociation of aromatic ketyls and pinacols.* Transactions of the Faraday Society, 1966. **62**(0): p. 918-925.
80. Turchi, C.S. and D.F. Ollis, *Photocatalytic degradation of organic water contaminants: Mechanisms involving hydroxyl radical attack.* Journal of Catalysis, 1990. **122**(1): p. 178-192.
81. Dai, L., Y. Xu, Y. He, J.-Y. Gal, and H. Wu, *A comparative study on the electrochemical properties of ring-substituted polyanilines.* Polymer International, 2005. **54**(9): p. 1256-1261.

82. Dai, X., M. Xie, S. Meng, X. Fu, and S. Chen, *Coupled systems for selective oxidation of aromatic alcohols to aldehydes and reduction of nitrobenzene into aniline using CdS/g-$C_3N_4$ photocatalyst under visible light irradiation.* Applied Catalysis B: Environmental, 2014. **158–159**: p. 382-390.

83. Moreira, N.F.F., J.M. Sousa, G. Macedo, A.R. Ribeiro, L. Barreiros, M. Pedrosa, J.L. Faria, M.F.R. Pereira, S. Castro-Silva, M.A. Segundo, C.M. Manaia, O.C. Nunes, and A.M.T. Silva, *Photocatalytic ozonation of urban wastewater and surface water using immobilized $TiO_2$ with LEDs: Micropollutants, antibiotic resistance genes and estrogenic activity.* Water Research, 2016. **94**: p. 10-22.

84. Sampaio, M.J., M.J. Lima, D.L. Baptista, A.M.T. Silva, C.G. Silva, and J.L. Faria, *Ag-loaded ZnO materials for photocatalytic water treatment.* Chemical Engineering Journal, 2016.

85. Sampaio, M.J., C.G. Silva, A.M.T. Silva, and J.L. Faria, *Kinetic modelling for the photocatalytic degradation of phenol by using $TiO_2$-coated glass raschig rings under simulated solar light.* Journal of Chemical Technology & Biotechnology, 2016. **91**(2): p. 346-352.

86. Comparelli, R., E. Fanizza, M.L. Curri, P.D. Cozzoli, G. Mascolo, R. Passino, and A. Agostiano, *Photocatalytic degradation of azo dyes by organic-capped anatase $TiO_2$ nanocrystals immobilized onto substrates.* Applied Catalysis B: Environmental, 2005. **55**(2): p. 81-91.

87. Marques, R.R.N., M.J. Sampaio, P.M. Carrapiço, C.G. Silva, S. Morales-Torres, G. Dražić, J.L. Faria, and A.M.T. Silva, *Photocatalytic degradation of caffeine: Developing solutions for emerging pollutants.* Catalysis Today, 2013. **209**: p. 108-115.

88. Gibot, P., F. Schnell, and D. Spitzer, *Enhancement of the graphitic carbon nitride surface properties from calcium salts as templates.* Microporous and Mesoporous Materials, 2016. **219**: p. 42-47.

89. Kumar, S., A. Baruah, S. Tonda, B. Kumar, V. Shanker, and B. Sreedhar, *Cost-effective and eco-friendly synthesis of novel and stable N-doped ZnO/g-$C_3N_4$ core-shell nanoplates with excellent visible-light responsive photocatalysis.* Nanoscale, 2014. **6**(9): p. 4830-4842.

90. Xin, G. and Y. Meng, *Pyrolysis Synthesized g-$C_3N_4$ for Photocatalytic Degradation of Methylene Blue.* Journal of Chemistry, 2013. **2013**: p. 5.

91. Mane, G.P., D.S. Dhawale, C. Anand, K. Ariga, Q. Ji, M.A. Wahab, T. Mori, and A. Vinu, *Selective sensing performance of mesoporous carbon nitride with a highly ordered porous structure prepared from 3-amino-1,2,4-triazine.* Journal of Materials Chemistry A, 2013. **1**(8): p. 2913-2920.

92. Jakob, M., H. Levanon, and P.V. Kamat, *Charge Distribution between UV-Irradiated $TiO_2$ and Gold Nanoparticles: Determination of Shift in the Fermi Level.* Nano Letters, 2003. **3**(3): p. 353-358.

93. Linic, S., P. Christopher, and D.B. Ingram, *Plasmonic-metal nanostructures for efficient conversion of solar to chemical energy.* Nature Materials, 2011. **10**(12): p. 911-921.

94. Mulvaney, P., *Surface Plasmon Spectroscopy of Nanosized Metal Particles.* Langmuir, 1996. **12**(3): p. 788-800.

95. Nassau, K., *Experimenting with Color*. 1997: F. Watts.

96. Silva, W.L.d., M.A. Lansarin, and C.C. Moro, *Síntese, caracterização e atividade fotocatalítica de catalisadores nanoestruturados de $TiO_2$ dopados com metais.* Química Nova, 2013. **36**: p. 382-386.

97. Thomas, J. and M. Yoon, *Facile synthesis of pure $TiO_2$(B) nanofibers doped with gold nanoparticles and solar photocatalytic activities.* Applied Catalysis B: Environmental, 2012. **111–112**: p. 502-508.

98. Reynolds, J.L., K.R. Erdner, and P.B. Jones, *Photoreduction of Benzophenones by Amines in Room-Temperature Ionic Liquids.* Organic Letters, 2002. **4**(6): p. 917-919.

99. Silva, R.S. and D.E. Nicodem, *Deuterium isotope effects on the photoreduction of 9,10-phenanthrenequinone and benzophenone by 2-propanol.* Journal of Photochemistry and Photobiology A: Chemistry, 2008. **194**(1): p. 76-80.

100. Ke, X., X. Zhang, J. Zhao, S. Sarina, J. Barry, and H. Zhu, *Selective reductions using visible light photocatalysts of supported gold nanoparticles.* Green Chemistry, 2013. **15**(1): p. 236-244.

101. Sarmah, P.P. and D.K. Dutta, *Chemoselective reduction of a nitro group through transfer hydrogenation catalysed by $Ru^0$-nanoparticles stabilized on modified Montmorillonite clay.* Green Chemistry, 2012. **14**(4): p. 1086-1093.

102. Wen, B., J. Ma, C. Chen, W. Ma, H. Zhu, and J. Zhao, *Supported noble metal nanoparticles as photo/sono-catalysts for synthesis of chemicals and degradation of pollutants.* Science China Chemistry, 2011. **54**(6): p. 887-897.

103. Ke, X., S. Sarina, J. Zhao, X. Zhang, J. Chang, and H. Zhu, *Tuning the reduction power of supported gold nanoparticle photocatalysts for selective reductions by manipulating the wavelength of visible light irradiation.* Chemical Communications, 2012. **48**(29): p. 3509-3511.

104. Herrmann, J.-M., *Heterogeneous photocatalysis: fundamentals and applications to the removal of various types of aqueous pollutants.* Catalysis Today, 1999. **53**(1): p. 115-129.

105. Niyaz A. Mir, A.K., A. A. Dar and M. Muneer, *Photocatalytic Study of Two Azo Dye Derivatives, Ponceau Bs and Reactive Blue 160 in Aqueous Suspension of $TiO_2$: Adsorption Isotherm and Decolorization Kinetics* International Journal of Innovative Research in Science, Engineering and Technology, 2014. **3**(2): p. 9333-9348.

106. Sugali, H.N., B.K. Kakati, and A. Verma, *Accelerated solar photocatalytic degradation of phenol using titanium dioxide.* Journal of Environmental Research And Development Vol, 2009. **3**(3).

107. Wakeham, R.J., J.A. Morris, and J.M.J. Williams, *Alternative Hydrogen Source for Asymmetric Transfer Hydrogenation in the Reduction of Ketones.* ChemCatChem, 2015. **7**(24): p. 4039-4041.

108. Dong, G., Y. Zhang, Q. Pan, and J. Qiu, *A fantastic graphitic carbon nitride ($g$-$C_3N_4$) material: Electronic structure, photocatalytic and photoelectronic properties.* Journal of Photochemistry and Photobiology C: Photochemistry Reviews, 2014. **20**: p. 33-50.

109. Zhou, X., G. Liu, J. Yu, and W. Fan, *Surface plasmon resonance-mediated photocatalysis by noble metal-based composites under visible light.* Journal of Materials Chemistry, 2012. **22**(40): p. 21337-21354.

110. Soares, O.S.G.P., M.F.R. Pereira, J.J.M. Órfão, J.L. Faria, and C.G. Silva, *Photocatalytic nitrate reduction over Pd–Cu/$TiO_2$.* Chemical Engineering Journal, 2014. **251**: p. 123-130.

111. Jiang, F., T. Yan, H. Chen, A. Sun, C. Xu, and X. Wang, *A g-$C_3N_4$–CdS composite catalyst with high visible-light-driven catalytic activity and photostability for methylene blue degradation.* Applied Surface Science, 2014. **295**: p. 164-172.

112. Xu, Y. and W.-D. Zhang, *CdS/g-$C_3N_4$ Hybrids with Improved Photostability and Visible Light Photocatalytic Activity.* European Journal of Inorganic Chemistry, 2015. **2015**(10): p. 1744-1751.

113. Woan, K., G. Pyrgiotakis, and W. Sigmund, *Photocatalytic Carbon-Nanotube–$TiO_2$ Composites.* Advanced Materials, 2009. **21**(21): p. 2233-2239.

# Appendix A

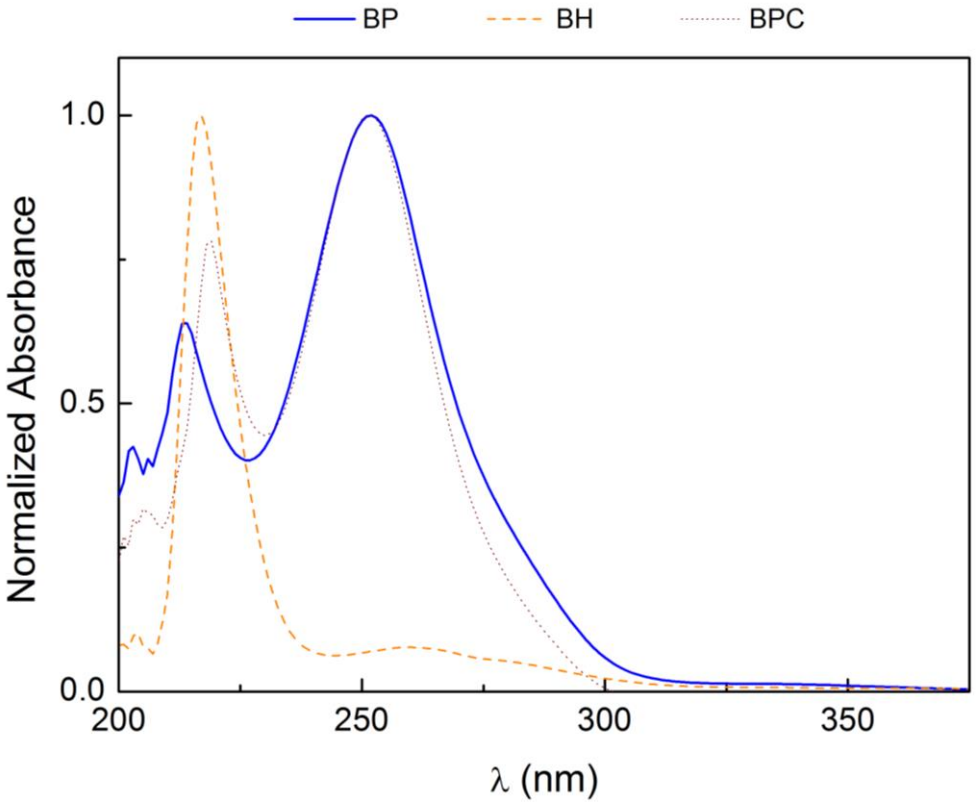


**Figure A.1 -** Ultraviolet-Visible spectra of Benzophenone (solid), Benzhydrol (dashed) and Benzopinacol (dotted), obtained using a JASCO V-560 UV–vis spectrophotometer and using iPrOH as solvent.

Even though the BP and BPC UV-Vis spectra are very similar, especially around the 250 nm zone, these had different residence times for the HPLC and so these were easily distinguishable.

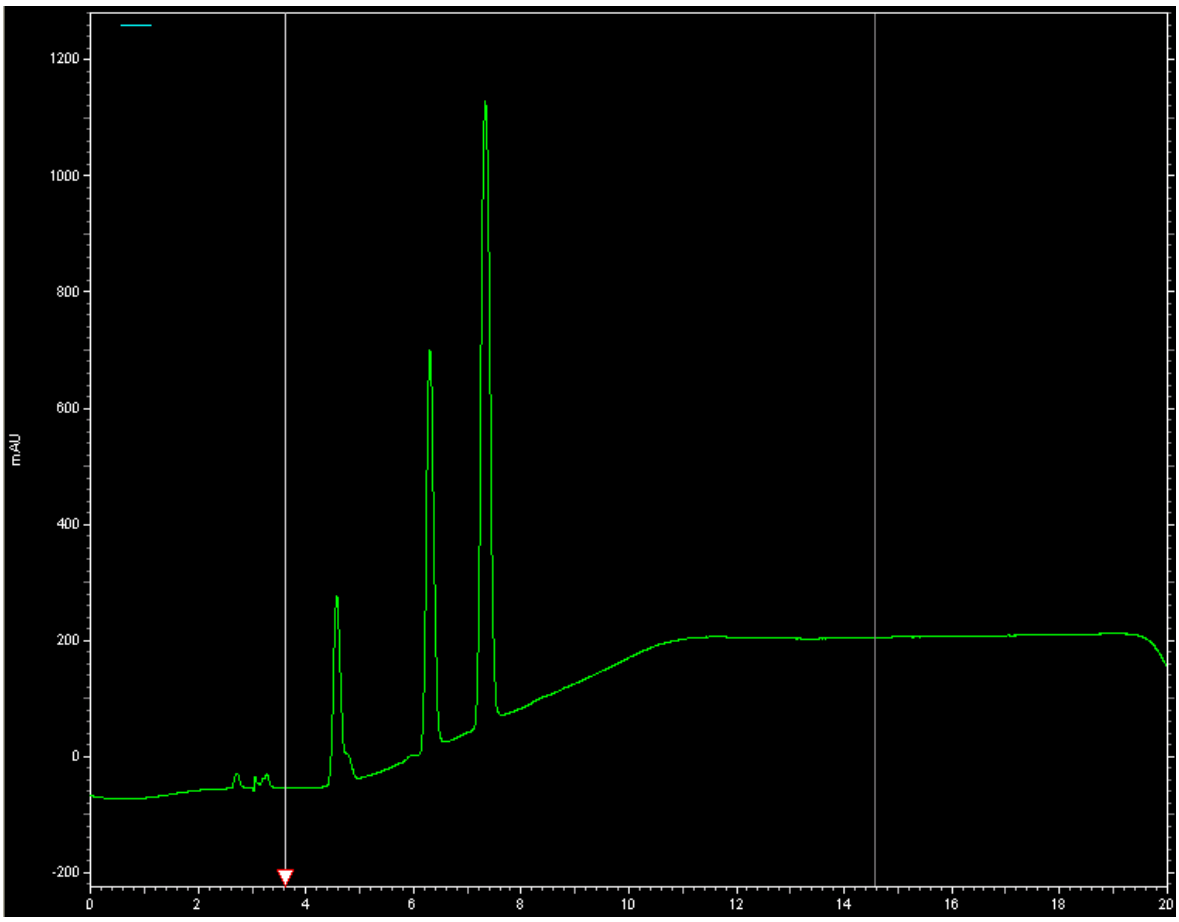


**Figure A.2** - Obtained chromatogram, with detector response (in a.u.) versus time (in minutes) from the HPLC at 202 nm from the 15 minute sample of the photocatalytic reaction with $TiO_2$ P25 load of 1 g $L^{-1}$ under simulated solar light, with a KOH concentration of 5 mM and having iPrOH as solvent.

As can be observed from the chromatogram of Figure A.2, the peak at 4.56 minutes corresponds to the BH, at 6.31 minutes the BP and 7.29 the BPC. Unidentified products were detected in the elution from 0 to c.a. 5 minutes.

# Appendix B

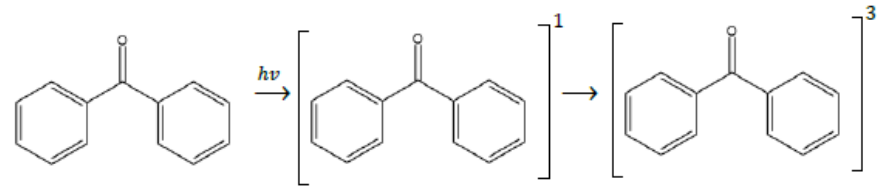


B.1)

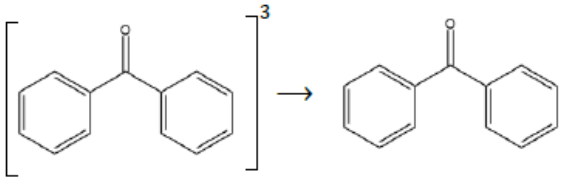


B.2)

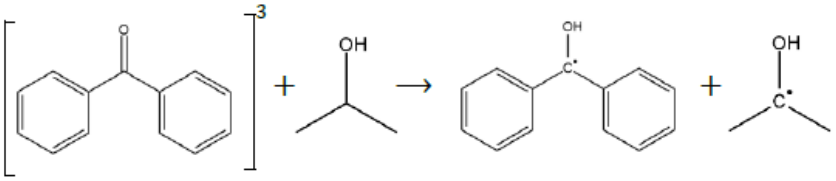


B.3)

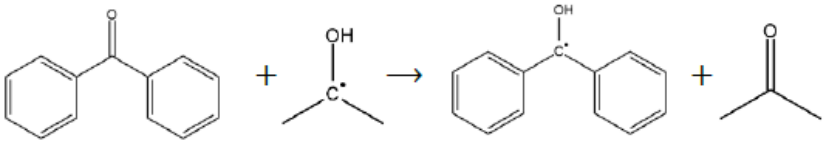


B.4)

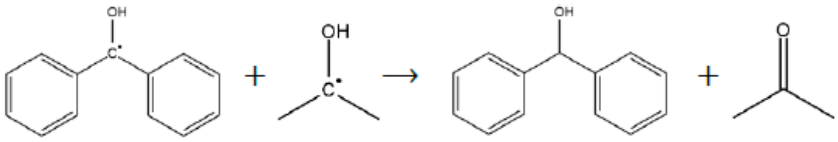


B.5)

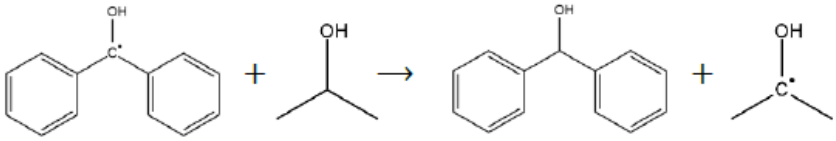


B.6)

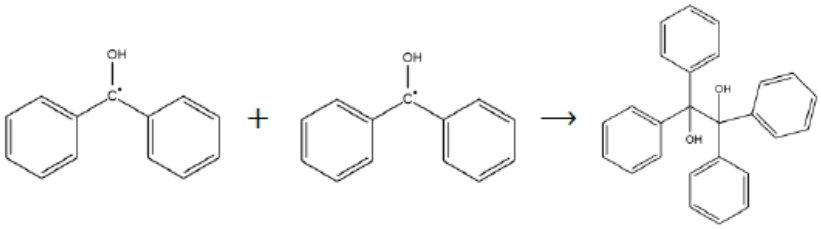


B.7)

**Figure B.1 -** Proposed photochemical mechanism for the photoreduction of BP for the attainment of BH, adapted from different sources [11, 13-15, 21].

The proposed mechanism for the photochemical reduction of BP with iPrOH as solvent under UV irradiation is as follows, according to different sources [11, 13-15, 20, 21].

Tipically, the substrate has all of its electrons on the minimal energetic level, the so called “ground state”, where the electrons that are held in the highest energy molecular orbital are most likely to be excited by a photon. So, a photon is absorved by BP if it possesses energy matching or greater than the orbital energy of that molecule, causing the molecule to jump from a low energy state to a higher energy orbital, while conserving angular spin momentum (Eq. B.1). This is known as an electronically excited singlet state. This is not its lowest energy state, so several things can happen from this instance. Either it returns to its ground state (Eq. B.2), a process known as fluorescence, or its spin direction may change, forming a triplet state BP (Eq. B.1). This is known as intersystem crossing.

From here, hydrogen abstraction from iPrOH by the triplet state BP to yield the diphenyl ketyl and dimethyl ketyl radicals happens (Eq. B.3), followed by radical transfer from the dimethyl ketyl radical to BP to yield acetone and another diphenyl ketyl radical (Eq. B.4). However, hydrogen abstraction from the triplet state substrate may also happen from the dimethyl ketyl, giving diphenyl ketyl radical and acetone. Finally, dimerization of diphenyl ketyl radicals to yield BPC (Eq. B.7) or new hydrogen abstraction of this radical from the alchohol (Eq. B.6) or its dimethyl ketyl radical (Eq. B.5) may succeed, producing BH [15, 20].